Chapter 3

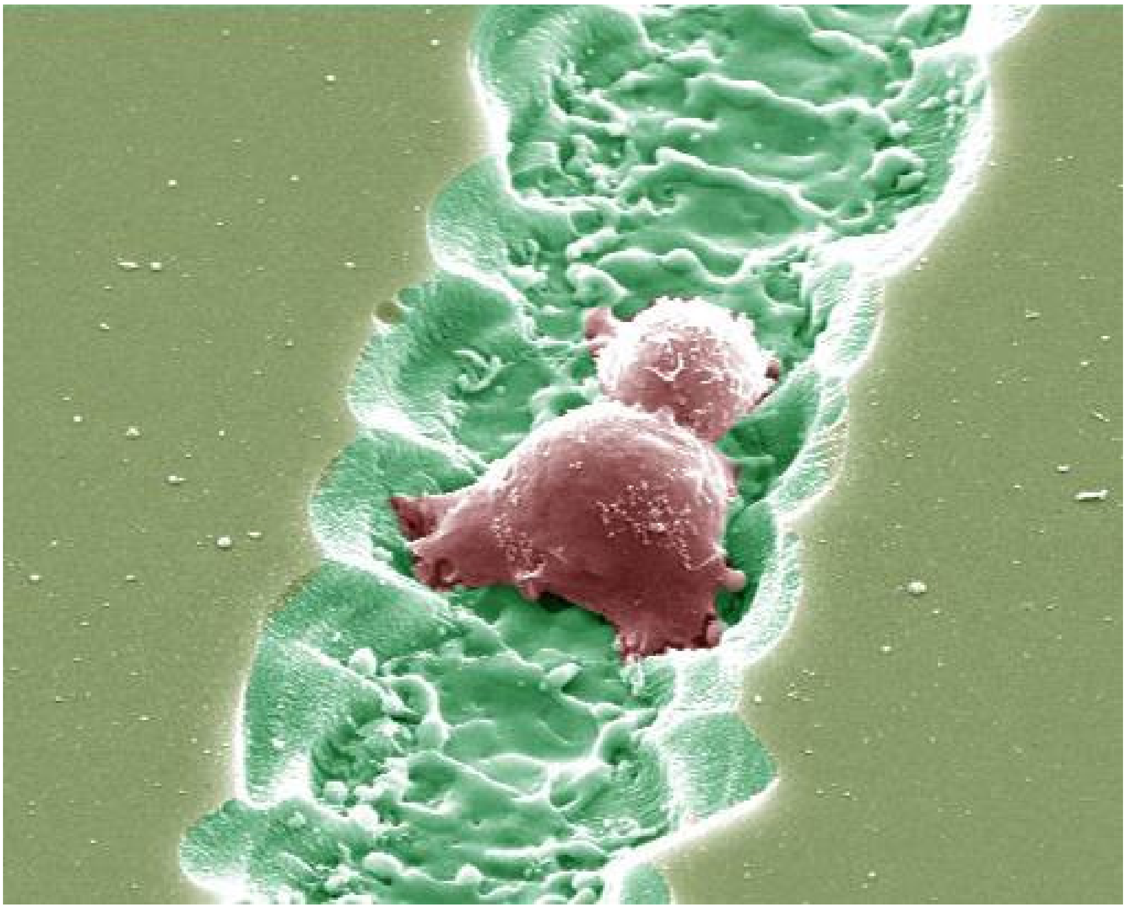

Micropatterning of cell attachment on pSi films by direct laser writing

Chapter outline

In the previous chapter, we demonstrate that functionalisation with PEG chains on pSi surface produced excellent low-fouling surfaces that discourages cell attachment. Here, we describe a selective removal of these PEG functionalised surface by direct laser writing in order to designate and specify PEG exclusion areas on the surfaces. On a single pSi surface, PEG exclusion patterns restrict cell attachment to the designated location while regions untouched by the laser writing strongly discourage cell attachment. The laser writing technique was found to be useful in controlling and directing cell attachment and adhesion patterns on the surface. This in turn permits us to achieve 2-dimensional cell-surface guiding, a key feature for bioimplant and bioreactor technology. We also found that if the duration of the laser ablation is extended, deep trenches can be etched from the pSi layer. Cells seeded into these trenches were observed to form multilayers. This stacking of cells is a step towards mimicking tissue organisation *in vivo*.

In this chapter, direct laser writing will be performed for:

3.1 Directing neuronal cell adhesion on pSi by direct laser writing

3.2 Formation of narrow strips of cells on pSi micropatterns

3.3 Reconstruction of artificial 3-dimensional hepatocyte cords on micropatterned pSi

3.1 Directing neuronal cell adhesion on pSi films by direct UV laser writing

The ability to control the growth of mammalian cells on semi-conducting materials promises the construction of new biochips for neuron functional assays and is motivating the present work. Recent advancements in microfabrication and micropatterning technologies for cell culture have spurred the development of chip-based multiplexed biosensors and biochips[1, 2]. Microengineering has also enabled fundamental studies in cell biology and has contributed to the understanding of critical issues such as modulation of cell-to-substrate adhesion and cell migration[3]. The same technology is also aspiring to become an invaluable tool for applications such as tissue engineering and cell culture analogs[1, 3, 4]. A variety of methodologies are available for the generation of patterned substrates for cell culture with the purpose of mediating selective adhesion of cells. These methods include lithographical tools such as photolithography[5], soft lithography[6, 7] and dip-pen nanolithography[8]. The popular method of microcontact printing in particular, allows the definition of different surface chemistries on a flat substrate featuring, for example, fouling and non-fouling regions or displaying a variety of functionalities[7, 9, 10]. An alternative approach consists of the application of networks of microfluidic channels over a substrate for the delivery of bioactive species which adsorb to the locations on the substrate exposed to the channel grid or for the delivery of a curable fluid[11]. In recent studies, excimer laser ablation has been used in a top-down fashion to ablate a non-fouling graft polymer of polyethylene glycol (PEG) to reveal an underlying cell growth conducive plasma polymer surface[12, 13].

The properties of pSi make it a promising substrate for cell culture given its biocompatibility, biodegradability[14-16], the tunability of pore size from the nano to the microscale[17, 18] and its rich surface chemistry[19]. Several recent reports focus on the *in vitro* testing of pSi biomaterials[14, 20-22]. Over the last decade, the optical properties of this nanostructured material have also attracted significant attention for applications covering a breadth of areas like photonics[23] and biosensors[17, 24-26]. The diversity of pSi architectures also holds considerable promise for tissue engineering where a porous scaffold is required to accommodate and guide the growth of mammalian cells in three dimensions[4, 27]. Exciting new pathways to the development of biologically enabled or enhanced sensors (e.g. neuronal biosensors or biomaterials) could be explored through control of the interface of bacterial or mammalian cells and pSi.

In this first section, we demonstrate that porous silicon films can be ablated by the pulsed nitrogen laser of a commercial MALDI mass spectrometer. With MALDI, it was possible for us to monitor the extent of the ablation at real-time by observation of the generated mass spectra. The extent of laser-induced ablation was found to depend on the doping level and surface chemistry of the porous silicon film. Using direct laser writing with or without a mask, micropatterns were generated on the porous silicon surface. These micropatterns were subsequently used to guide the growth of mammalian cells including neuroblastoma (Figure 3.1). Excellent selectivity of cell growth towards the laser-ablated regions was established.

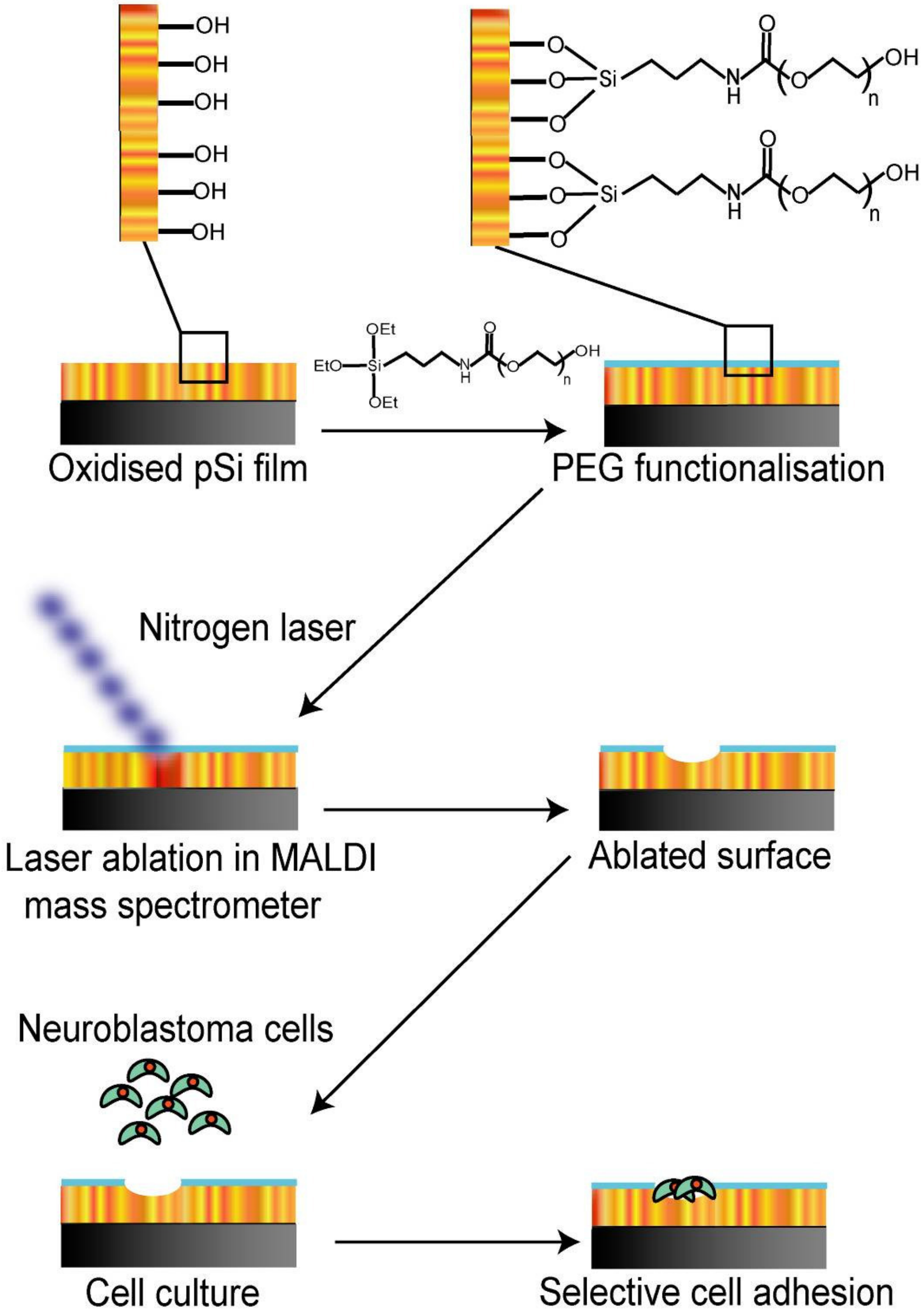

Figure 3.1 - Schematic summary of the experimental approach used in this work. Non-fouling PEG chains (n = 4-7) were grafted onto the surface of oxidised porous silicon. A nitrogen laser was used to ablate regions on the porous film. Neuroblastoma cells were shown to selectively grow on the ablated regions.

Coffer and coworkers utilised microcontact printing to spatially direct the formation of mesoporous silicon and its subsequent calcification[28]. However, post-etch lithographical patterning of porous silicon is difficult to achieve without the destruction of the porous layer[29] due to mechanical stressed experienced by the pores. Laser ablation on the other hand has been successfully employed not only to prepare porous silicon[30, 31], but also to decorate pSi post-etch with photoluminescent quantum dot arrays for the purpose of generating waveguides[32, 33].

Inspired by these studies, this work illustrates a novel approach towards micropatterning for cell culture, which is summarised in figure 3.1. The surface of porous silicon was first functionalised with N-(triethoxysilylpropyl)-O-polyethylene oxide urethane to render the surface non-fouling. This surface was subsequently ablated with the nitrogen laser of a commercial MALDI mass spectrometer to form microscale patterns on the surface. The surface topography of these ablated patterns was studied by AFM in conjunction with SEM. The surface chemistry and composition was studied by diffuse reflectance infrared spectroscopy. Finally, SK-N-SH human neuroblastoma cells were found to selectively adhere on ablated areas of the micropatterns.

3.1.1 Methods and materials

pSi samples were prepared from p-type (boron-doped) silicon wafers with (100) orientation and resistivity of 0.0005-0.001Ω·cm (Virginia Semiconductors). Samples were etched in a 3:1 (v/v) solution of 49% aqueous HF/EtOH for 1 min at a constant current density of 133 mA/cm^2. The resulting pSi layers were 1.5cm in diameter and approximately 2 µm thick (determined by SEM). After etching, the samples were rinsed with methanol, acetone and dichloromethane and were dried under a stream of N_2. The freshly etched pSi surfaces were oxidised by exposure to ozone at a flux of 8 g/hr for 20 mins and subsequently rinsed with CH_2Cl_2 and EtOH.

3.1.1.1 pSi surface functionalisation

The oxidised samples were immersed in 50 mM of N-(triethoxysilylpropyl)-O-polyethylene oxide urethane in toluene for 18 hours at 70°C. The PEG functionalised pSi surfaces were then rinsed extensively with toluene, CH_2Cl_2 and EtOH and subsequently dried under a stream of N_2.

3.1.1.2 Diffuse reflectance infrared fourier transform spectroscopy

Analysis of surface chemistry via IR spectroscopy was performed with using a Nicolet Avatar 370MCT equipped with a Smart Diffuse Reflectance accessory at a resolution of 4cm^{-1}.

3.1.1.3 Nitrogen laser ablation

Laser ablation was carried out using the pulsed (4 nsec) nitrogen laser (337 nm, 90 µJ per pulse) of a Micromass MALDI-LR mass spectrometer. Ablation was carried out at a pulse rate of 10 Hz. The mass spectrometer was also used to monitor the intensity of the PEG containing ions produced during the ablation. Upon attenuation of this peak, the motorized stage of the instrument was used to move the sample underneath the laser beam in increments of 20 µm between each ablation cycle. The patterned pSi surfaces were rinsed with EtOH and dried in a stream of N_2.

3.1.1.4 AFM measurements

AFM was performed to characterise the aftermath effects of the laser ablation on the porous silicon. The images were acquired on a Nanoscope E microscope (Veeco Corp.) operating in contact mode. Image processing was done using Nanoscope v5.12 software.

3.1.1.5 SEM analysis

For cell fixation, the pSi surfaces were carefully removed from the 6-well plate after the incubation time. They were rinsed once with PBS and fixed in 3.7% formaldehyde in PBS for 10 mins at room temperature. Subsequently, the surfaces were washed again twice in PBS and incubated in turn in 50%, 75% and 100% EtOH for 10 mins. The surfaces were then washed twice in PBS, incubated in hexane, dried in the laminar airflow, and subsequently coated with platinum[34]. SEM was performed on a Phillips XL30 field emission scanning electron microscope with an acceleration voltage of 10kV to visually observe the effects of the laser ablation on the different modified pSi surfaces.

3.1.1.6 Cell culture on micropatterns

Prior to cell culture, pSi surfaces were extensively washed with EtOH and dried with N_2 in a laminar flow hood. The patterned pSi wafers were transferred onto sterile 6-well plates. 2 mls of SK-N-SH neuroblastoma cells were grown to confluence and then immediately seeded onto the pSi samples at a density of about 1.46 x 10^7/ml. The pSi wafers were incubated at 37°C for 24h. At the end of the incubation time, 10 µl of 15 mg/ml of FDA in acetone and 2 µl of EtBr were added to the media and the wafers were incubated at room temperature for 10 mins. Cell cultures on the pSi surface exhibiting the ablated square patterns were stained by adding 4 µl of 3,3'-dioctadecyloxacarbocyanine (DiO) and incubated on the surface overnight. The media from the overnight culture was subsequently removed and 50 µl of 0.002% propidium iodide (PrI) in PBS was added. The surface was incubated at room temperature for 5 mins. The pSi sample was subsequently removed from the wells and gently rinsed with 1X PBS. Cell attachment was observed using a Leitz fluorescence microscope.

3.1.2 Results and Discussion

3.1.2.1 Preparation and characterisation of pSi films

Mesoporous pSi films were prepared by electrochemical anodisation as described earlier[25]. Freshly etched pSi displayed diffuse reflectance spectra consistent with a hydride terminated surface (figure 3.2 (a)). It is an unstable surface in aqueous environment (undergoing rapid oxidation and pore corrosion) and is therefore often stabilised by surface oxidation. Upon exposure to ozone, the bands corresponding to bending and stretching modes of Si-H_x (~2100cm^{-1}) were replaced by a peak at 1080 cm^{-1} and a shoulder at 1160 cm^{-1} attributed to an asymmetrical Si-O-Si and Si-OH stretching modes, respectively (Fig. 3.2 (b) and (c))[17, 35, 36]. Further stabilisation of the surface against hydrolytic attack in aqueous medium was achieved by wet chemical silanisation using a PEG terminal silane. PEG chains were used to impart non-fouling properties to the pSi matrix. Silanisation with N-(triethoxysilylpropyl)-O-polyethylene oxide urethane led to the appearance of two peaks at 2940 and 2890 cm^{-1} corresponding to aliphatic v(C-H) stretches. In addition, the silanised pSi surface exhibited a peak at 1710 cm^{-1} attributed to the urethane C=O vibration and a second one at 1540 cm^{-1} assigned to the urethane C-N bond. The shoulder at 3350 cm^{-1} to the right of the broad interference peak centred at 3590 cm^{-1} is indicative of hydrogen bonded O-H.

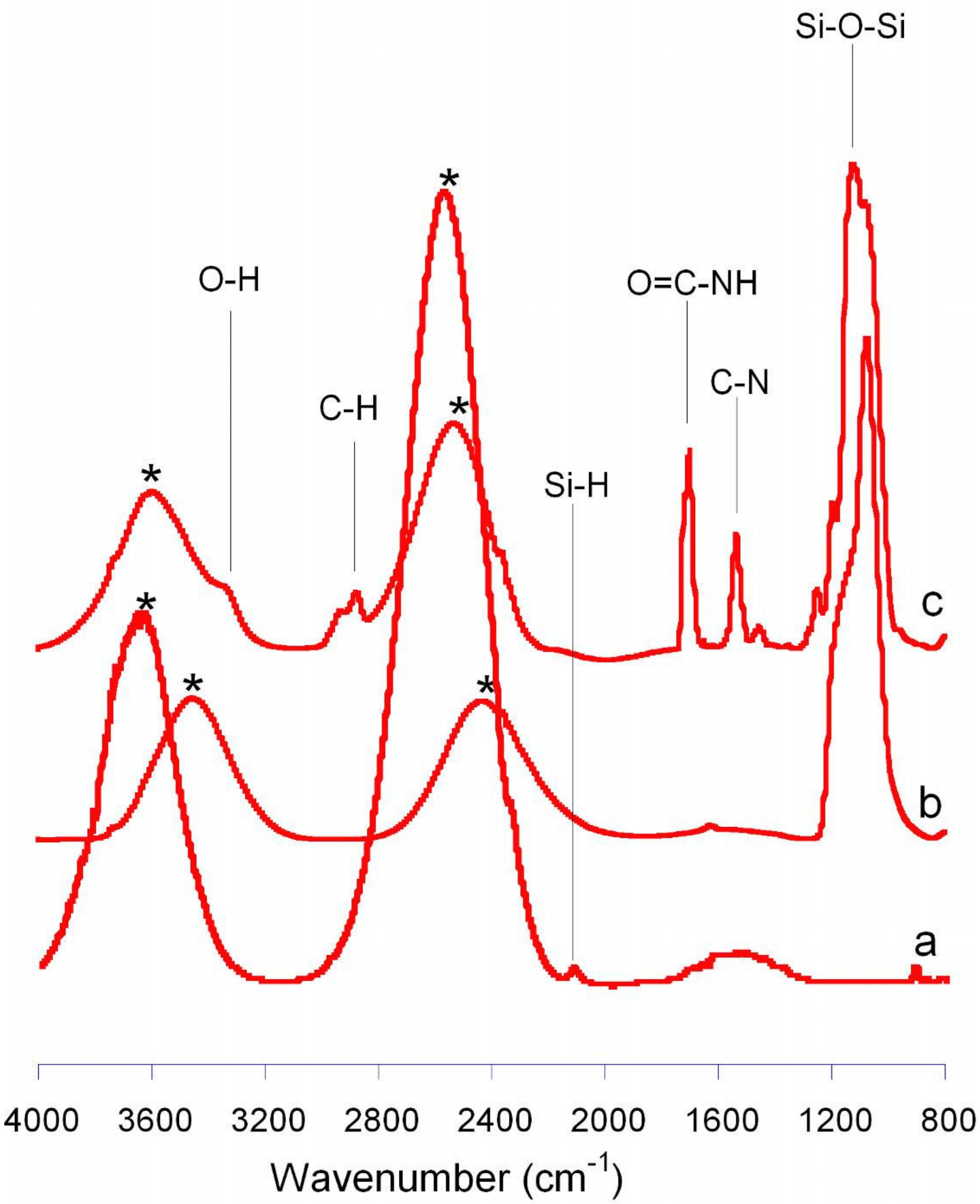

Figure 3.2 - Diffuse reflectance IR spectra of pSi. (a) Freshly etch pSi, (b) Ozone oxidised pSi and (c) PEG functionalised pSi. The bands under the asterisks correspond to IR reflective interference effects with evenly sized broad peaks[35].

3.1.2.2 Nitrogen laser ablation of pSi films

Laser ablation was performed by exposure of pSi films to the nitrogen laser (337 nm) of a commercial MALDI mass spectrometer with a beam width of 80 µm and a power density per pulse of 1.79 J/cm^2. We observed that the nitrogen laser was able to ablate the pSi surface, however ablation under the same conditions was not observed when applied to a single crystalline silicon wafer. Furthermore, laser ablation was found to be dependent on the doping level and the surface chemistry of pSi. For instance, on highly doped, low resistivity p-type pSi (< 0.001 Ω·cm) extensive ablation was observed whilst only minimal ablation was found on pSi films made from higher resistivity p-type wafers (1-5 Ω·cm), again under the same experimental conditions. Figure 3.3 shows SEM and AFM images of low resistivity pSi (freshly etched, ozone oxidised and PEG functionalised) after dragging a nitrogen laser beam across its surface. Ablation was extensive on freshly etched pSi leading to a 40-50 µm wide ablated trench. Laser ablation is facilitated by the high absorption cross-section of pSi in the UV range[37, 38]. However, the same laser power only introduced <10 µm in diameter and roughly circular craters on oxidised pSi (compare figure 3.3 (a) and (b)). Interestingly, ablation on the PEG functionalised surface again led to the formation of a continuous trench which was shallower than the trench observed after ablation on the freshly etched pSi (50 nm versus 400 nm as determined from AFM cross-sections), yet had about the same width (40 µm). At this point, we can only speculate that the different ablation behaviour on these three surfaces is due to slight changes in thermal conductivity[39]. The thermal conductivity of highly doped p-type porous silicon is typically about half that of bulk silicon. However when the porous silicon is oxidised the thermal conductivity decreases drastically since the formed oxide layer creates heat barriers which act as thermal resistors[40].

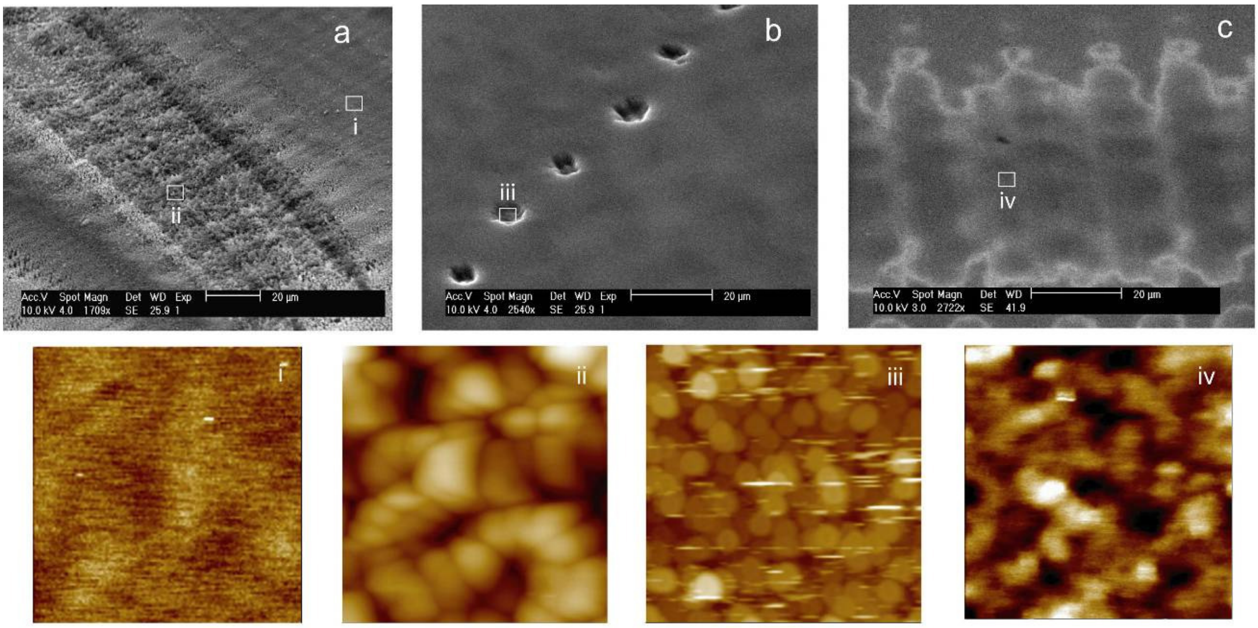

Figure 3.3 - Nitrogen laser ablation on porous silicon of < 0.001 Ω·cm resistivity. SEM of laser ablated area on (a) freshly etched pSi, (b) ozone oxidised pSi and (c) PEG functionalised pSi (scale bar = 20 µm). Contact mode AFM analysis of the surfaces were taken in regions marked by a white square in the SEM; (i) AFM image of freshly etched pSi surface, (ii) within ablated region of freshly etched surface, (iii) within a pit formed from ablation on ozone oxidised surface and (iv) within an ablated region on PEG functionalised pSi. All AFM images are 1 µm in lateral scale. Z scale for (i)-(iv) is (i) 5 nm, (ii) 150 nm, (iii) 100 nm and (iv) 8 nm.

Contact mode AFM was employed to further investigate the surface morphology the laser ablated regions. Figure 3.3 (i) shows an AFM image of the mesoporous structure of the supported pSi film. After laser ablation, the porosity has changed significantly and the oxidation of the pSi was likely to have occurred as well. As figures 3.3 (ii-iv), taken in the centre of an ablated trench or crater, demonstrate laser ablation leads to the formation of 200-500 nm sized globular silicon nanoparticles. These are presumably the products of laser induced silicon melting and re-solidification and similar features have recently been described for laser ablated pSi[33].

3.1.2.3 Monitoring the ablation process by mass spectrometry

A major advantage of utilising the MALDI mass spectrometer in the current study is the inherent ability to monitor the laser ablation process in real-time by observation of the generated mass spectra. The mass spectral data, produced during the ablation process, showed spectra characteristic of PEG functionality with well-defined, uniform peak separations of 44 m/z (corresponding to ethylene glycol oligomers). Furthermore, by monitoring the decline in intensity of these PEG spectral fingerprint regions, it is possible to determine the required duration of laser exposure during the course of patterning (figure 3.4). We found that 30 sec was generally sufficient to completely attenuate the PEG signal in the mass spectrometer.

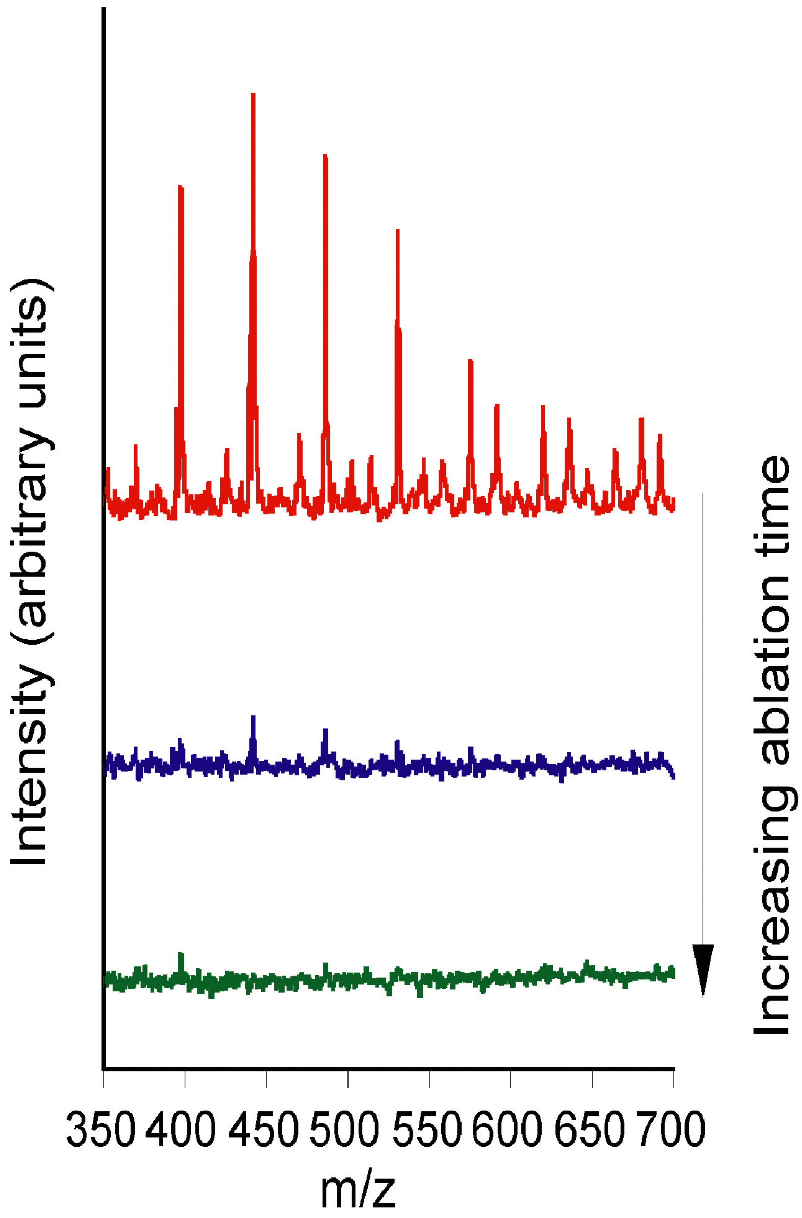

Figure 3.4 - MALDI mass spectra obtained during the course of laser ablation on PEG functionalised pSi. The red, blue and green spectras were taken at the 4 seconds, 12 seconds and 30 seconds intervals respectively.

3.1.2.4 Micropattern formation by direct laser writing on pSi

Microscale patterns were generated on the PEG functionalised surface using two different methods. Firstly, linear patterning was achieved by incremental movement of the motorised stage holding the functionalised pSi sample (figure 3.5 (a)). The resulting ablated lines were observed to be 40-80 μm in width. Secondly, grid patterns (figure 3.5 (b)) were generated in an inverse fashion by guiding the laser beam over a mesh mask whilst the functionalised pSi wafer was held stationary.

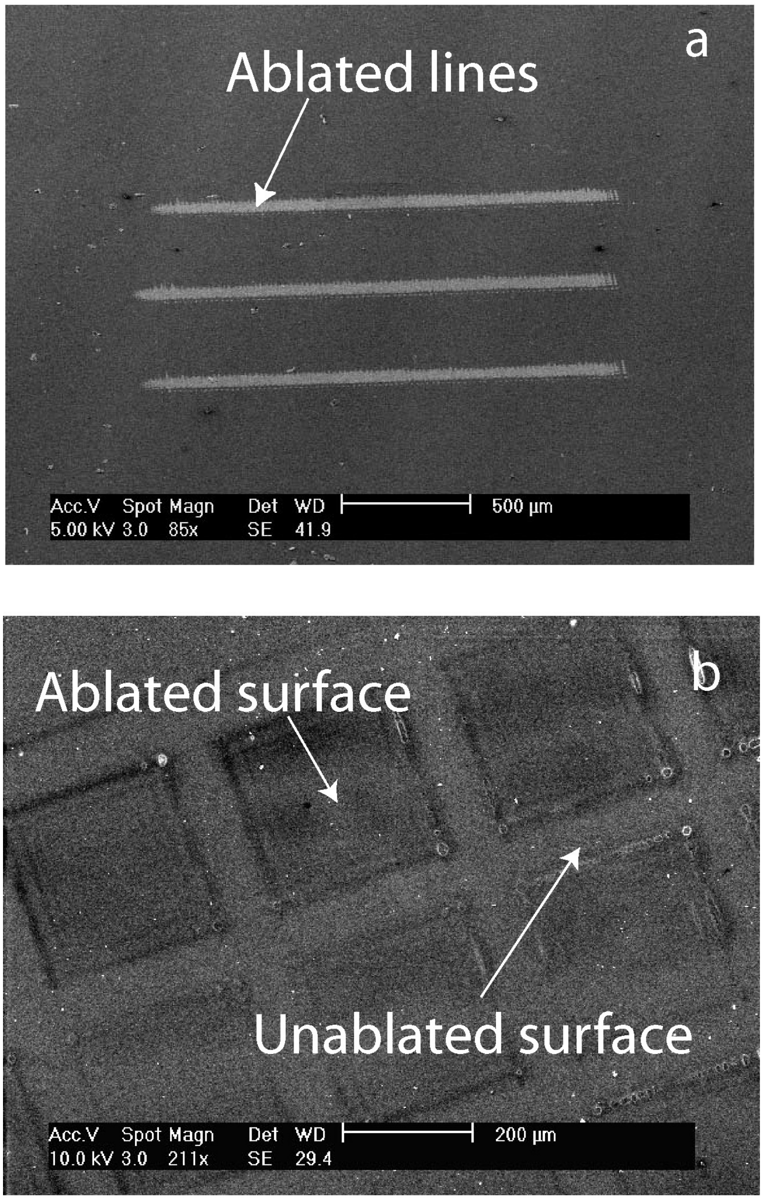

Figure 3.5 - Scanning electron microscopy micrographs of PEG functionalised pSi films after laser ablation using the nitrogen laser of a MALDI mass spectrometer. Laser ablation was used to generate parallel lines (a) and grid patterns (b).

Nitrogen laser interrogation of pSi was used by Siuzdak et al for the purpose of mass spectrometry and has led to a popular laser desorption mass spectrometry approach termed desorption/ionisation on silicon (DIOS)[37, 38]. In DIOS, pSi is used instead of an organic matrix to absorb the laser energy and enable controlled energy transfer to analytes adsorbed within the porous layer. However, the concept of utilising a UV laser for surface micropatterning of pSi is novel and to the best of our knowledge has not been attempted previously. The approach described here is particularly distinctive because the laser of a commercial MALDI mass spectrometer was used for laser writing permitting the ablation process to be monitored and controlled in situ via the time-of-flight mass spectrometer function.

3.1.2.5 Cell culture experiments on laser-patterned pSi

SK-N-SH human neuroblastoma cells were chosen in this instance as a model cell culture for the generation of patterns of primary neurons on laser-patterned pSi[41, 42]. The application of the micropatterning method described here to neuronal cells can potentially be adapted for the study of neural networks or developmental cues in neurons and can lead to an improved comprehension of learning and memory. Neuroblastoma cells are known to be adhesive to a variety of substrate surfaces[41, 42] and are commonly used as an experimental model in neurobiology to study cell differentiation [43, 44], signaling and ion channel function[45-47].

After 24h incubation of neuroblastoma cells on PEG functionalised pSi, cells were stained with either a combination of fluorescein diacetate (FDA) and ethidium bromide (EtBr) or 3,3’-dioctadecyloxacarbocyanine (DiO) and propidium iodide (PrI). Cell attachment was completely absent, showing that the terminal PEG functionalisation did render the porous silicon surface as non-fouling. Limited cell attachment was observed on oxidised pSi. Meanwhile, extensive cell attachment was found on non-porous regions of the PEG functionalised silicon wafers (figure 3.6 (a)). After pattern formation via the nitrogen laser, cell attachment was restricted to the ablated areas on the sample (figure 3.6 (b)-(d)). In figure 3.6 (b), a confluent layer of stained cells was observed to attach, subsequently filling the laser-written lines. Cells appeared healthy, with well spread processes and exhibited the characteristic teardrop shape of typical neuroblastoma morphology[48, 49]. Notably, a few live cells were observed outside of the ablated region, connected to the confluent cell layer, but these cells had a distinguished rounded appearance with no notable processes. No dead cells (indicated by red fluorescence) were observed on any of the investigated surfaces. In addition, micropatterned grids (figure 3.6 (c)) were also defined by laser ablation. The cross-line pattern consisted of ablated lines (figure 3.6(c)) or ablated squares (figure 3.6 (d)). Neuroblastoma cell growth was again observed to occur exclusively within the ablated regions.

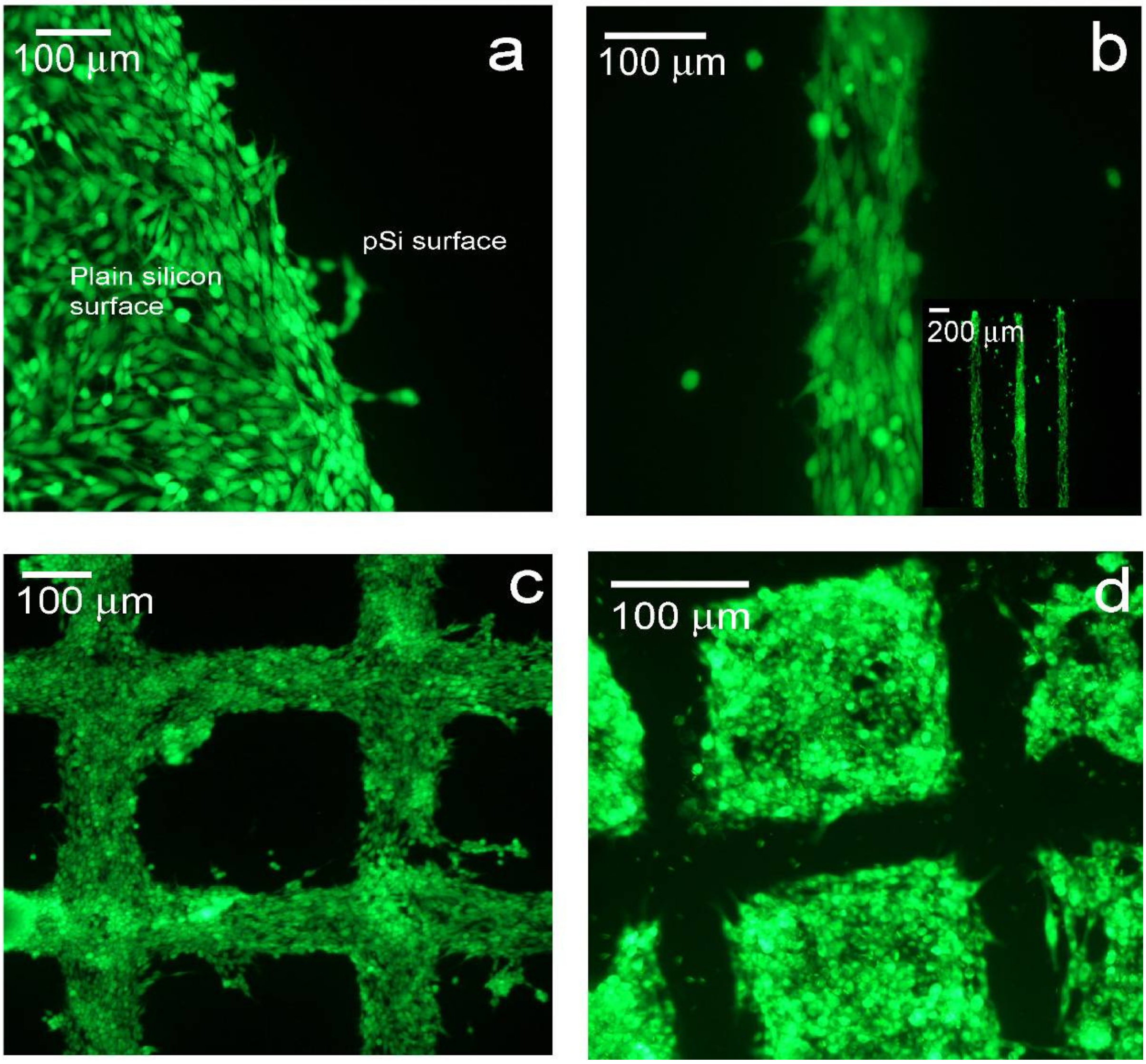

Figure 3.6 - Fluorescence microscopy images of FDA/EtBr stained SK-N-SH neuroblastoma cells growth on patterned pSi samples after 24 hours incubation: (a) confluent cell growth was observed on non-porous (plain) PEG functionalised silicon surface. Cells were absent on PEG functionalised pSi. (b) Selective cell adhesion to ablated lines and multiple parallel lines (inset). (c) Selective cell growth to cross-line pattern with ablated line and (d) selective cell growth to ablated squares of an inverse cross-line pattern (cells, in this case, were stained with DiO/PrI).

This patterning approach was also successfully applied to other mammalian cell lines like rat adrenal pheochromocytoma (PC12) and human embryonic kidney epithelial cells (HEK293) (see figure 3.7 (a)). Furthermore, we found that intact cell layers could be lifted off the ablated regions (figure 3.7 (b)-(c)) demonstrating that our approach of micropatterning biodegradable materials also holds promise for tissue engineering, for example where viable cultured cell sheets need to be detached from their substrate surface on demand before transplantation. The detachment of cell sheets from the substrate surface had already been demonstrated in the past by thermoresponsive polymeric surfaces such as poly(*N*-isopropylacrylamide) (Poly-NIPAM)[50-52]. These polymers will change its hydrophobicity at different temperatures, i.e. the surfaces are hydrophobic at 37° that will promotes cellular adhesion while at 32°, the surfaces swells and becomes hydrophilic. This shift in hydrophobicity and swelling will induce cells to be detached from the surface. Here, using laser ablation on pSi, we had demonstrated another mechanically non-destructive alternative for detaching cell sheets on micropatterned surface.

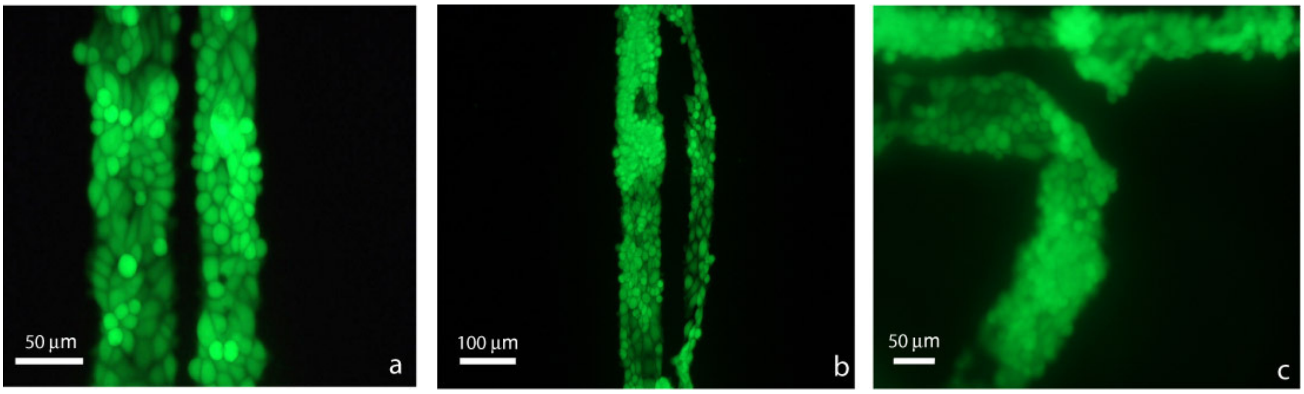

Figure 3.7 - Fluorescence microscopy images of FDA/EtBr stained PC12 cells grown for 24h on laser patterned pSi samples: (a) two parallel lines, (b) cell sheet partly twisted upon gentle rinsing with PBS and (c) PC12 cell sheet peeled from the laser ablated line after more extensive rinsing with PBS.

3.1.3 Conclusions

The pulsed nitrogen laser of a commercial MALDI mass spectrometer was employed to microengineer cellular adhesion on mesoporous silicon films. The laser writing process was studied by AFM and SEM and could be monitored in-situ by mass spectrometry. The studies discovered that direct laser writing on pSi can successfully generate cellular micropatterns and the subsequent exploitation of this technique may be applied to cell-based biosensors, biochips and tissue engineering, in particular cell harvest technology or cell sheet engineering. Silanisation of the porous silicon surface with a terminal PEG functionality was effective in suppressing the growth of mammalian cells. Cell growth closely followed the laser written micropatterns. Given that our preliminary cell culture studies were successfully performed on neuroblastoma cells, further investigations of neuronal processes including their development and intercellular communication are now feasible.

3.2 Engineering of 1-2 cell wide monolayer cell sheets in pSi trenches

There are many studies focusing on the interfacing of a living tissue network with silicon-based devices[53-59]. The main motivation for interfacing cell or tissue with silicon is that silicon-based technology has already been well-established and readily accessible for designing and patterning micron-scale topographical/chemistry features. These devices are often used on cell/tissue for viability and toxicology screening[58, 59] and also for producing miniaturized neuronal based transistors that can activate or inactivate signals at will from the interface[53, 54, 60].

One of the most important aspects during interfacing of cells and silicon surface is control of the propagation and the general cellular orientation on the surface. This is important, especially in the context of neuron transistors where the orientation, the extent of neuronal growth cones and level of the interconnectivity between neurons are instrumental towards achieving a high quality neuro-electronic interface. Controlling the propagation and orientation of cells on surfaces was often achieved by chemical and topographical cues on the surface[61-63]. However, some of the major weaknesses with chemical guidance is the inability for cells to correctly follow bends and corners on the pattern and cellular projections often bridge between the lanes of growth[53]. These bridging between cellular projections can be undesirable where orderly cell patterns is required[64]. Topographical guiding had fared much better for directing cell orientation than chemical[63]. However, the fabrication of these surfaces can be time consuming and expensive.

In section 3.1, we have demonstrated that by exposing the pSi surface to a pulsed nitrogen laser, it is possible to direct cell growth on the laser-patterned surfaces. pSi is an attractive material for tailoring neuron-silicon interface as its chemistry and fabrication methodologies had already been well addressed. One added asset of pSi films is their porous microarchitecture that can permit the flow of fluid or diffusion of viable biomolecules throughout the system. In the previous section, lines were ablated using a MALDI laser with an 80 μm beam-width, and these lines were about 60-80 μm in width (see figure 3.7). These lines gave rise to a 4-6 cell wide sheet upon incubation with an adherent cell suspension. Interestingly, while the ablation by the MALDI laser had removed/displaced only 40 nm from the pSi film, this was deemed sufficient to alter the surface chemistry at the ablated site. Since the number of cells per column is dependent on the width of the line, it is, therefore, technically possible to reduce the number of cells per column by decreasing the width of the ablated lines. This narrowing of ablated lines on the surface can be applied to tailor 1-2 cell wide cell sheets on pSi films. These narrow cell sheets on the silicon surface can contribute greatly towards the realization of micron-size neuro-electronic interfacing devices[53, 54, 60].

Here, we report the machining of 25 μm wide ablation lines by direct laser writing with a microdissection microscope on pSi surface. As schematically shown in figure 3.8, lines ablated from the MALDI laser were 40-80 μm and these lines formed 6-8 cell wide sheets but if the lines were made narrower (25 μm), it is possible to engineer 1-2 cell wide cell sheets. These narrower lines can be used for directing the growth of narrow neuron and liver sheets. One major advantage of using the microdissection microscope is the capacity to fine-tune the width of the laser beam by mere adjustment of the aperture. Furthermore, as the laser from the microdissection microscope is more intense (300 μJ per pulse compared to the 90 μJ per pulse of that of the MALDI), it was possible to produce deeper trenches (5 μm). The depth of these trenches and the PEG moieties on unablated regions prevented cells from growing and propagating away off the micropatterns.

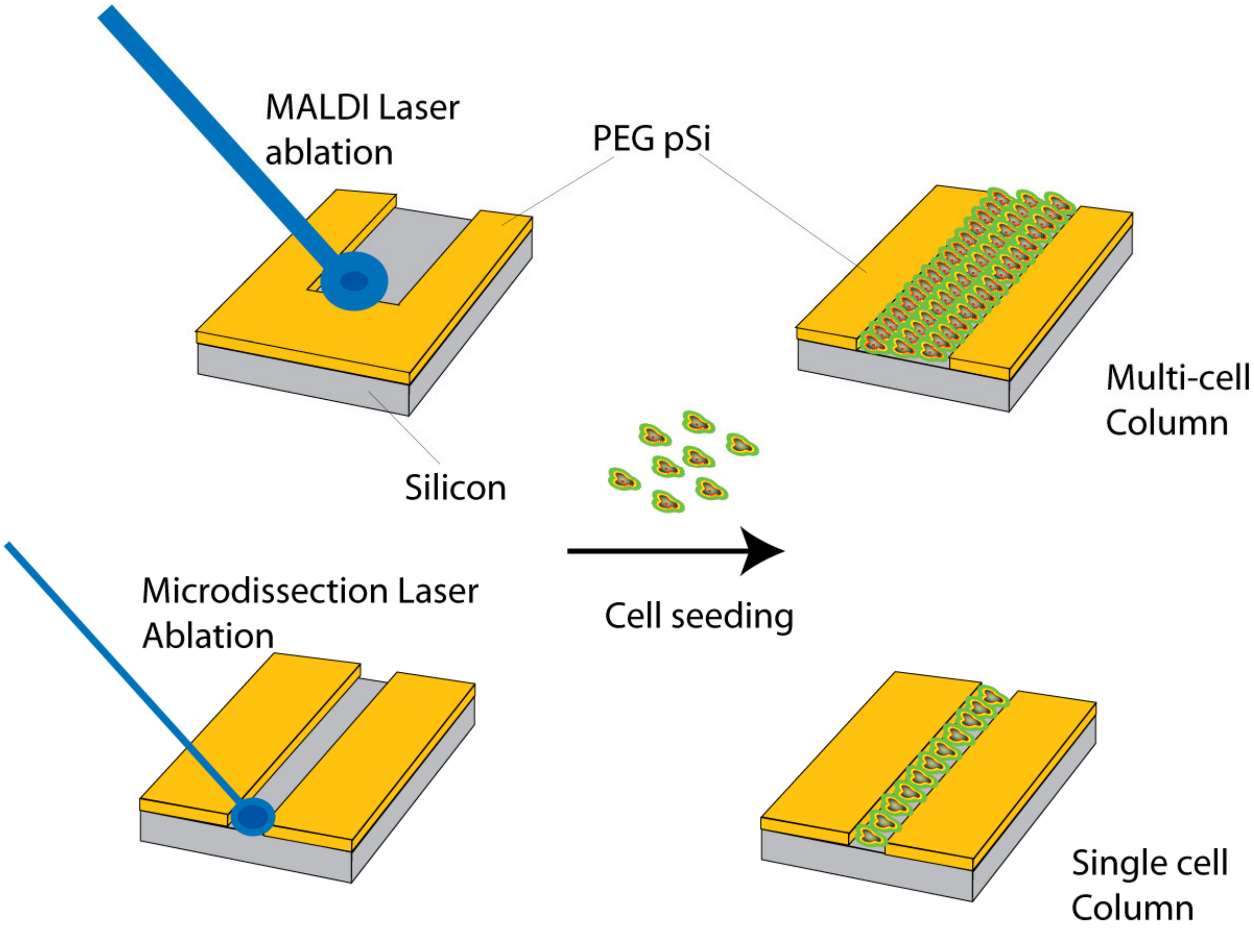

Figure 3.8 - The width of laser ablation influences the amount of cell attachment on the surface. By reducing the width of the laser beam, it is possible to tailor thin lines with approximately 25 µm in width and these thinner lines in turn allows for the patterning of single cell column on the pSi surface.

3.2.1 Methods and Materials

3.2.1.1 Microdissection laser ablation

After the pSi surfaces were fabricated (see Section 3.1.1) and functionalised with PEG silane (see section 3.1.2), the surfaces were extensively washed with EtOH and dried with N_2 in a laminar flow hood. The pSi surfaces were subsequently ablated with a 337 nm nitrogen laser (30 Hz, 4 ns pulse width, 75 kW beam intensity) from a laser microdissection microscope (Leica Microsystems) at Adelaide Microscopy. All settings for the ablation on the surface were specified and controlled by the LMD software that was attached to the microscope. The laser was first calibrated on the microscope to ensure that the lines drawn by the mouse on the monitor was identical with the lines ablated by the laser on the surface. To ablate narrow lines on the pSi surface, the software setting that controls power intensity were preset at 42and the speed of the ablation at 30-40 μm per second. A 10x objective lens was used for all surface ablation. Lines and circles of length ranging from were subsequently ablated by the laser. All lines were ablated 3 times repeatedly under this laser setting.

3.2.1.2 AFM measurements

AFM was perform to study the effects of the surface ablation and all images were acquired on a Nanoscope E microscope (Veeco Corp.) operating in contact mode. Image processing was done with Nanoscope v5.12 software.

3.2.1.3 SEM analysis

SEM analysis was performed on a Phillips XL30 field emission scanning electron microscope with an acceleration voltage of 10 kV and a capture angle of 80 degrees relative to the surface to observe the cross-section of the ablated trench on the pSi film.

3.2.1.4 Cell culture

Micropatterned pSi surfaces were first were rinsed with 95% EtOH and subsequently dried at room temperature in the laminar air flow. These surfaces were then aseptically transferred into sterile 6-well plates. The two different cell lines were used: SK-N-SH neuroblastoma and H4IIE hepatoma cells. For each cell line, a cell suspension at a density of 6.5 x 10^5 was seeded onto the surface. The surfaces were incubated at 37°C for 24 hours in filter sterilised Dulbecco's modified Eagle Medium (DMEM) that contains 10% (vol/vol) Fetal Bovine Serum (FBS), 50 IU/ml penicillin and 50 mg/ml streptomycin sulphate and the pH was adjusted to 7.2 with 0.1 M HCl.

3.2.1.5 Fluorescence microscopy

After 24h, 2 µg/ml of Hoechst 33342 dye was added to the culture wells in order to stain the cell nucleus and the wells were incubated at 37ºC for 30 mins. Subsequently, 10 µl of 15 mg/ml of FDA was added to the media and the wafers were incubated at room temperature for another 10 mins. The surfaces were then washed with PBS to remove non-adhering cells and fluorescence microscopy under the excitation wavelength of 270-380 nm and 495-552 nm were performed for both the Hoechst and the FDA stain, respectively, using a Leitz fluorescence microscope.

3.2.2 Results and discussion

3.2.2.1 Surface ablation via laser microdissection microscope

In contrast to the MALDI laser, the ablation patterns were accurately prescribed by the software prior to the ablation event on the laser microdissection microscope. Thus, ablated lines were more precise and the ablation time was much faster. Furthermore, it was also possible to assign many lines and circles simultaneously on the software that controlled the ablation while this was not possible from the MALDI setup.

However, while the MALDI laser ablation permits inherent monitoring of the ablation event at real time, this could not be achieved with the microdissection microscope. Yet we were able to visually observe plumes formed during the ablation of the silicon surface and these ablation plumes acts as indicators to the extent of the ablation. It is well documented that the colour of the plume during ablation of any given surface is dependent on a wide series of factors such as surface moiety[65] and certain atmospheric conditions[66]. During the ablation, the colour of the plumes observed when the pSi layer was generally orange, while the ablation on the bulk silicon surface would yield bluish white plumes. This visual observation of the plume colour was subsequently used as an indication of how far the ablation had occurred into the pSi layer.

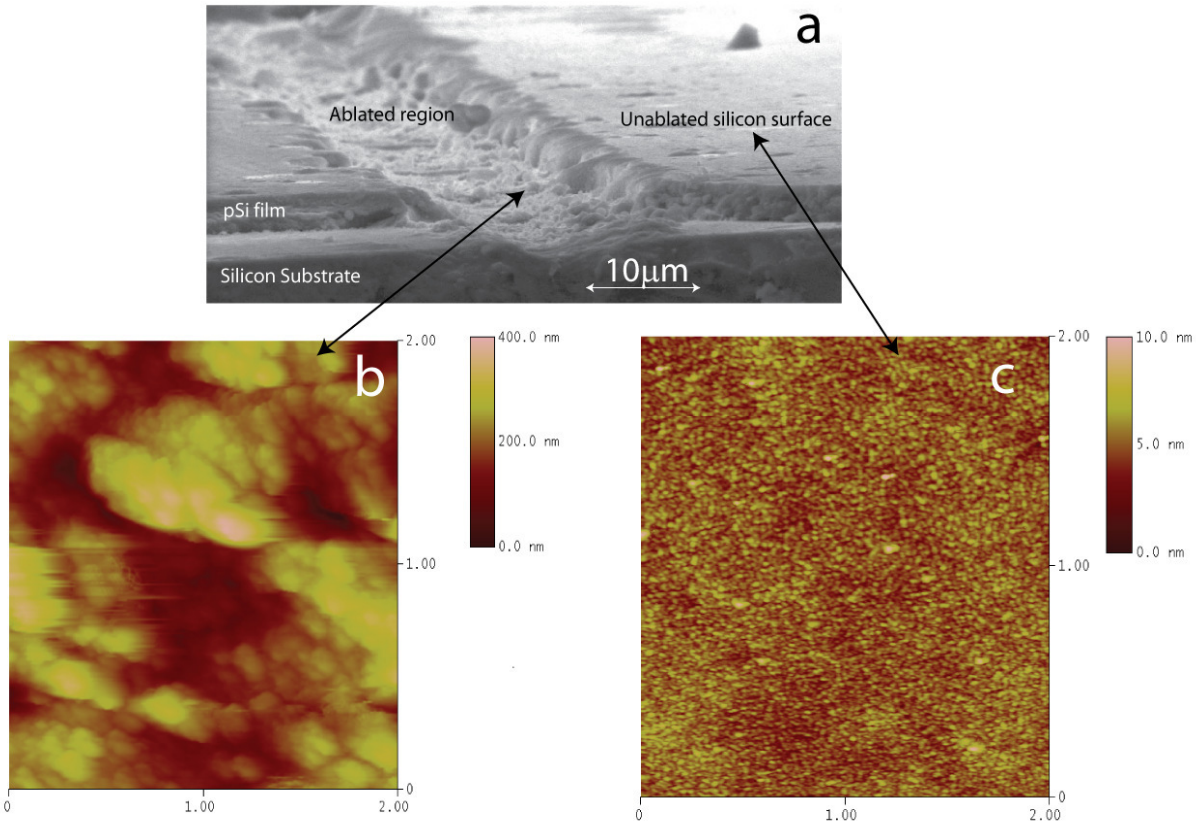

Figure 3.9 – (a) SEM of the ablated lines on the pSi surface. Note that the laser completely ablates into the pSi film. Film thickness of the pSi layer was measured at 4 µm. AFM analysis was also performed for (b) the ablated region and (c) region unablated by the laser.

As described in the experimental, all lines designated on the software were repeatedly ablated 3 times. After the third ablation, SEM was employed to investigate the morphology of the ablated lines on pSi surface. As shown in figure 3.9 (a), the SEM image of the ablated line revealed a trench of approximately 25 µm on the surface in width and the depth of the laser ablation was 5 µm. During ablation, the plume was observed to be orange in colour during the first 2 ablation runs and by the third ablation run, the plume colour had changed to a bluish white. Thus, by the observing the plume formed, we found that the ablating 3 times on a single line was sufficient enough to remove the entire pSi layer (4 µm thick). This SEM finding also coincides with our observation of the colour of the ablation plume during the laser ablation. From this, we conclude that the intensity of the laser ablation from the microdissection microscope was much higher compared to the MALDI laser, which could only remove about 40 nm of the pSi layer.

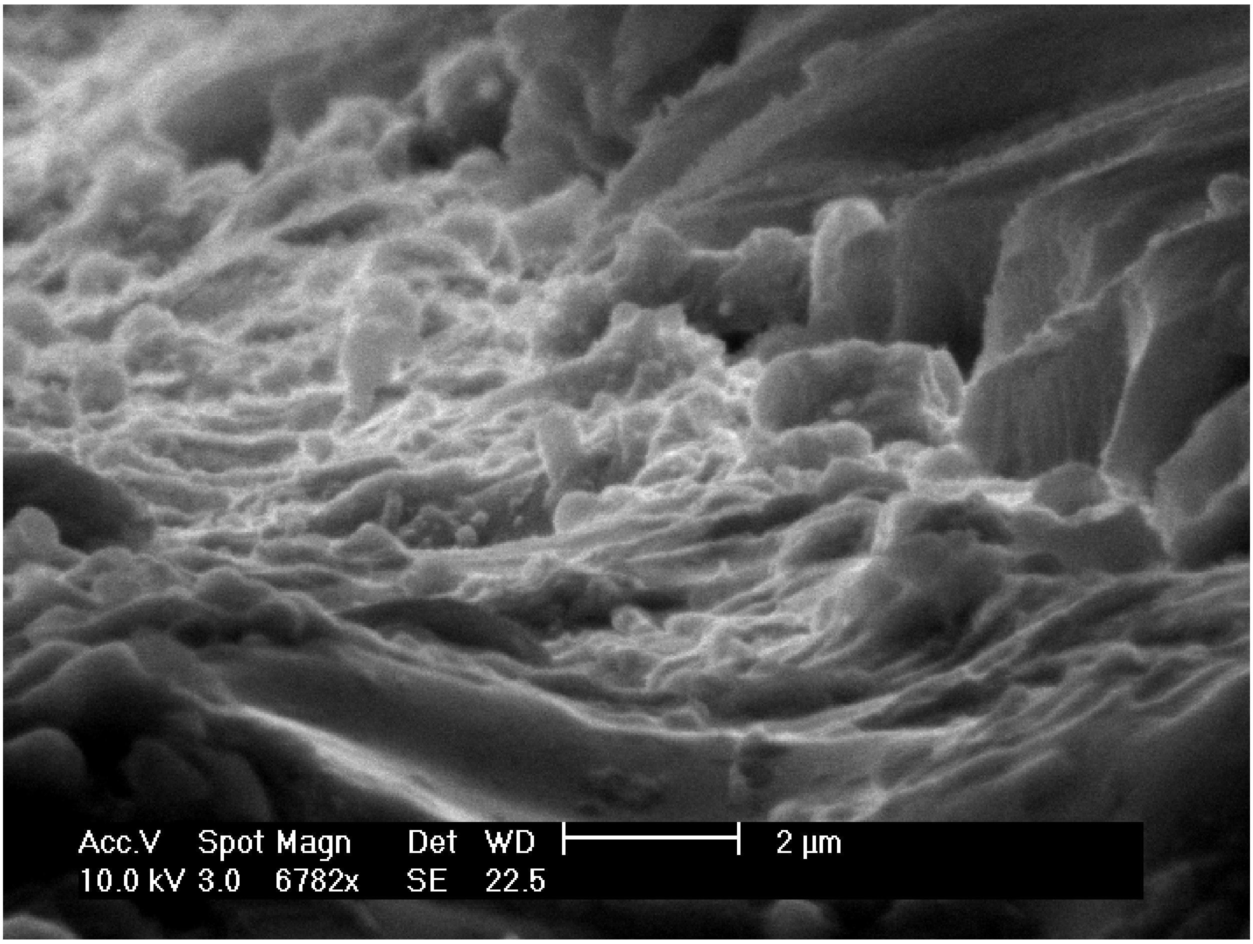

Figure 3.10 – SEM of the morphology of the ablated region on the PEG functionalised pSi surface by laser microdissection microscope

AFM and SEM analysis was also performed on the ablated region. As shown in figure 3.9 (b) and figure 3.10, the ablated surface had a rather rough and lumpy topography and this was presumably the result of laser induced melting and resolidification of the laser plume[67]. This extent of ablation was not observed for PEG functionalised pSi surface ablated by the MALDI. These observations strongly suggest that during ablation of surfaces at lower laser intensity, it is possible to influence the outcome of the ablation by modifying surface chemistry while the effects from surface chemistry is less felt at higher laser intensity .

3.2.2.2 Cell culture on narrow ablation lines

To evaluate cell response to these narrow lines, we decided to employ two different cell lines that have contrasting morphologies. Neuroblastoma cells typically exhibit a teardrop shape while H4IIE cells have a rounder cell morphology. Both cell types were seeded at equal density for a period of 24 hours. After the incubation time, nucleus (Hoechst) and cytoplasm (FDA) staining were performed to visualize the cells under the fluorescence microscope.

Figure 3.11 shows SK-N-SH neuroblastoma cells residing in lines ablated on PEG alkyl-silanised pSi that were 25 µm wide. As shown in figures 3.11 (a) and (b), it was possible for us to ablate either straight lines or circular patterns onto the surface by using the laser microdissection microscope. This further demonstrates the versatility of the microdissection microscope setup for surface patterning. Neuroblastoma cells generally formed a 1-2 cell wide cell sheets attaching on these lines and its cellular morphology were generally round due to densely packed nature within these cell sheets. Thus only a few cells were observed exhibiting the typical teardrop shape. The 1-2 cell wide cell sheets formed were within expectation as the width of these lines was around 25 µm while the typical width of an adherent neuroblastoma cell undergoing full neurogenesis on the surface was 10-15 µm[48, 68]. Very few cells were observed growing on the PEG functionalised pSi region that was untouched by the laser and those that were found on the unablated regions were often connected closely to the patterned cell column. These cells had a distinguished rounded appearance and tend to cluster together, thus confirming that PEG functionalised surface greatly discourages proper cell adhesion.

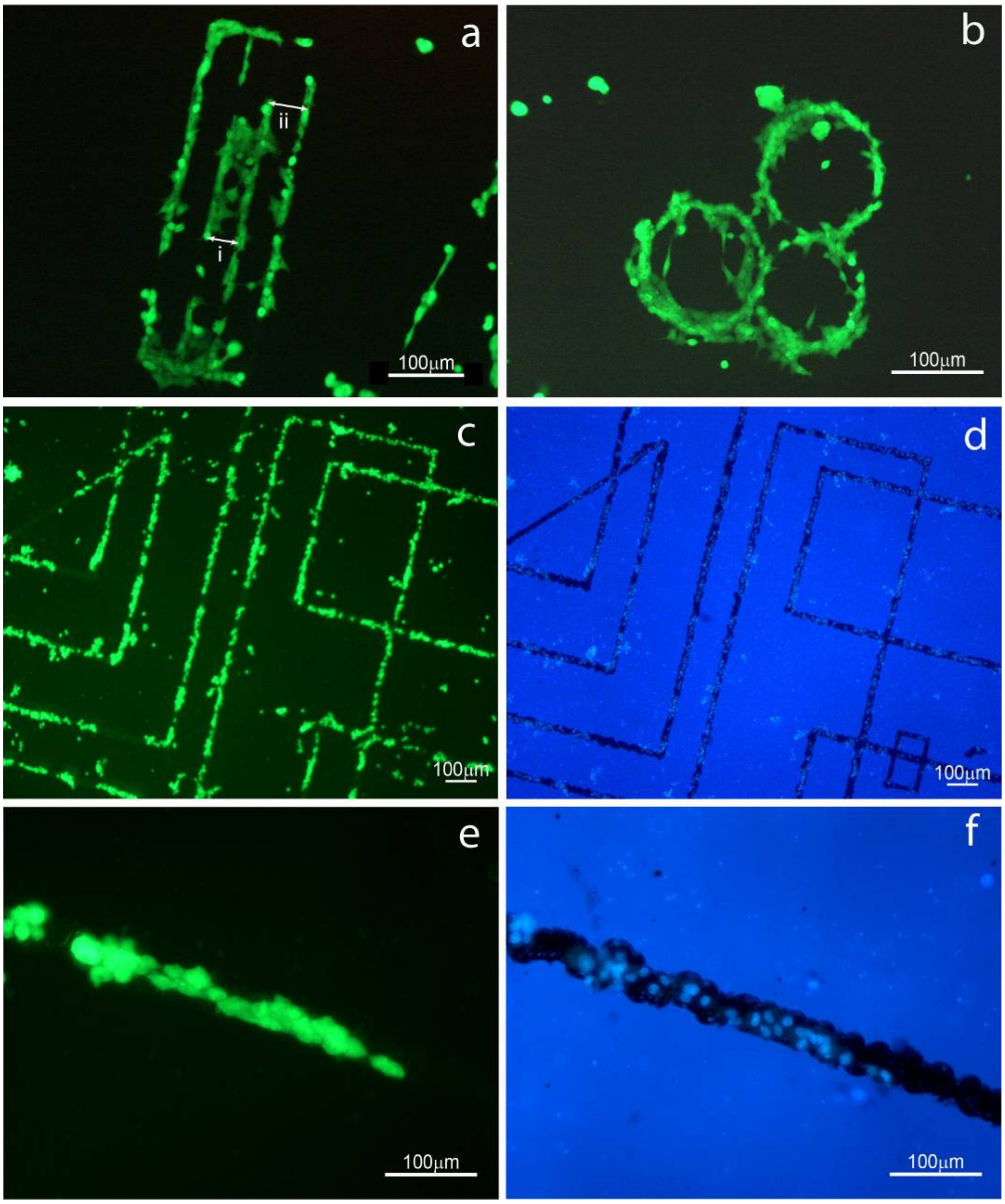

Figure 3.11 – Fluorescence microscopy of Hoechst/FDA stained SK-N-SH neuroblastoma cells growth on patterned pSi samples after 24 hours incubation: (a) FDA staining revealing cells attaching nearly exclusively on parallel lines and (b) circles. Cells were generally absent on PEG functionalised pSi surface untouched by the laser. (c) FDA and (d) Hoechst staining of cells growing on lines ablated on the pSi surface. The luminescence of the pSi region (in the blue channel) allows for the visualization of these ablated lines on the surface since the ablated region does not show luminescence Only columns of 1-2 cells were found residing on these narrow lines as shown by the FDA (e) and the Hoechst (f) stains.

Figure 3.11 (a) showed that neuroblastoma cell attachment was mostly confined along parallel straight lines within a 4-line rectangle. Interestingly, some of the attaching cells were observed overlapping between the 2 internal lanes within this rectangle. This overlapping of cell growth was not observed forming between the outer and the inner lanes and the segregation between the growing lanes was maintained. The distance apart measured between the 2 inner lanes was 40 µm (see figure 3.11 (a, i)) while the distance measured between the outer lane and one of the inner lines was 50 µm (see figure 3.11 (b, ii)). This suggests that overlapping growth between neuroblastoma attaching on parallel lanes with interspatial distance of 40 µm is high while this problem can be avoided by slightly increasing the distance between the growing lanes. It is also important to note that the depth of the trenches was only 5 µm and neuroblastoma cells sitting inside on these micropatterns may still be sufficiently elevated to extend their processes out of the trench to seek contact to other cells.

The ease and speed conferred by the microdissection microscope has allowed for faster patterning on the surface as compared to the MALDI laser. As shown in figure 3.11 (c), fluorescence images taken with a 4x objective revealed linear cell sheet attaching along numerous ablated lines on the pSi. Furthermore, when the pSi surface was imaged for Hoechst staining of the cell nucleus, the luminescence of the pSi region allowed for a clear visualization of these ablated lines on the surface (see figure 3.11 (d)). This is a useful optical property that permitted us to define cellular adhesion patterns. Higher magnification onto these ablated lines had indeed confirmed that the cell body and nucleus were mostly confined within the ablated lines (see figure 3.11 (e) and (f)).

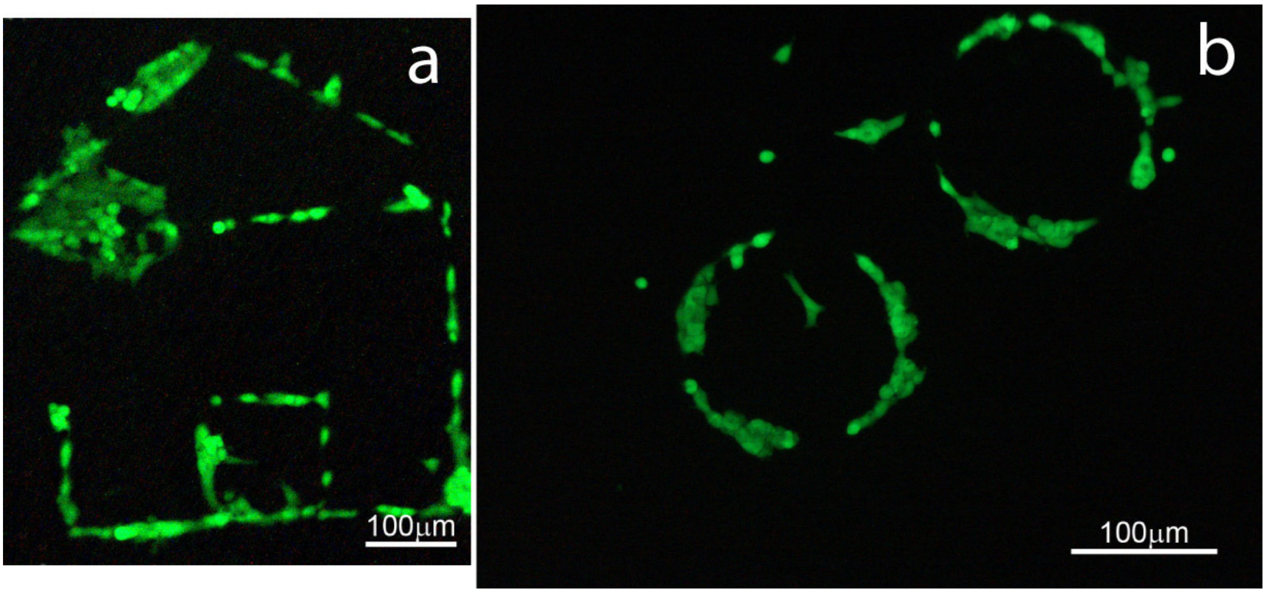

Figure 3.12 – Fluorescence microscopy of H4IIE cells preferentially adhering on the pSi micropatterns after 24 hours incubation: (a) cells attachment following the micropatterns to form an outline of a house and (b) outline of 2 circles.

H4IIE hepatoma cells seeded on these lines were also observed to adhere preferentially on the same 25 μm wide by 5 μm deep trenches (figure 3.12). The versatility of the microdissection microscope could be exploited to draw diverse shapes and patterns on the surface and cells were still observed attaching almost exclusively on the lines of these shapes. This was well illustrated in figure 3.12 (a) where the cells seeded over an ablated outline of a house closely follow the surface pattern. Interestingly, we noticed that H4IIE cells were much better at forming single cell column than neuroblastoma. We also observed more clustering over the lines and cells growing on these lines could be easily removed during PBS rinsing of the surface. Furthermore, we found that the number of cells attaching on non-ablated areas were observed to be much lower as compared to the neuroblastoma. These observations suggested that the H4IIE cells were more sensitive to the surface chemistry while the cellular attachments to the trenches were much weaker when compared to the neuroblastoma.

3.2.3 Conclusions

Micropatterning the pSi surface with the laser microdissection microscope is an excellent alternative to the MALDI setup described in the previous part. By ablating the surface with a finely focused laser, we were able to narrow lines 25 µm in width and depth. Using the software controlling the microdissection microscope, it was possible to accurately manipulate the shapes and length of the lines on the surface. Furthermore, by visually monitoring of the plume during the ablation, we were able to monitor the extent of the ablation.

Two different cells types were used on the trenches and both demonstrated to selectively grow on the ablated regions. The ablated lines were around 100 times deeper than those produced by the MALDI laser and this depth had contributed in confining the cells. As such, cell attachment was observed exclusively on these ablated lines. Possessing a good cell confinement was deemed crucial in this experiment as it was our intentions to engineer 1-2 cell wide cell sheet. As a result, the widths of these lines were only wide enough to accommodate for a 1-2 cell column. Furthermore, we also identified the interspatial distance between grow lanes required to avoid cell overlapping (> 40 µm) for neuroblastoma. This interspatial distance can be further narrowed theoretically by deeper ablated trenches that would effectively confine/conceal the cell column within the film. Finally, we have also noticed that neuroblastoma cells can adhere much better on the surface than H4IIE while the latter was more sensitivity to surface chemistry.

In summary, we have demonstrated that micropatterning of PEG functionalised pSi with the microdissection laser is a rapid surface patterning technique suitable for the generation of cell patterns that can produce 1-2 cell wide monolayer cell sheets. This technique can be used to precisely tailor cell growth on the surface. Our results have also confirmed the excellent flexibility in tuning pSi surface chemistry to control cell adhesion.

3.3 Reconstruction of artificial 3-dimensional hepatocyte cords on micropatterned pSi

The liver is the largest and one of the most important organs serving multiple essential functions in the human body. It comprises of a variety of epithelial and nonparenchymal cells and collectively, these cells form a 3-dimensional functional unit as illustrated in the schematic in figure 3.13. Epithelial cells, such as hepatocytes, make up the major cellular component of the liver. From the main blood veins, these cells extend out to assemble into cords with adjacent hepatocytes interconnected by lateral membranes. The regions within these cords are known as the sinusoids and these vascular spaces are responsible for the flow of nutrients and metabolite from the common vein. The intake of nutrients and metabolites from blood is in turn mediated by the fenestrated endothelium, a porous endothelium cell lining on the hepatocytes cord. In between the fenestrated endothelium and the hepatocytes lays a region comprising of random collagen fibers and fibroblast and this region is known as the space of Disse[69, 70]. Thin tubes known as Bile canaliculi formed between adjacent hepatocytes within the cord and function as a site for bile removal from the cells. These tubes will eventually converge to form the common hepatic duct that drains bile from the liver. Overall, the intrinsic cell–cell and cell–extra cellular matrix (ECM) interactions allow the hepatocyes in vivo to organise themselves 3-dimensionally and maintain the specific phenotypes and functions[71-73].

3-dimensional culture of hepatocytes has long been recognised as essential for the reconstruction of functional hepatic tissues in vitro. Hepatocyte aggregates known as hepatocyte spheroids[69, 74-78] are one of the more common 3-dimensional cell aggregates maintained in *in vitro* culture environment. These hepatocyte aggregates *in vitro* help maintain and extend the function of primary hepatocytes for prolong periods of time. Methods such as paper scaffolds[79], highly porous polymeric scaffolds[80, 81], 3-dimensional perfused microarray bioreactors[82] and collagen sponges[83] have been proposed for supporting these 3-dimensional aggregates. However, the major weakness is that while these aggregates are useful as bioartificial liver (BAL)[77, 78, 84, 85], their structures do differ significantly from those of the liver in vivo. In their natural environment, hepatocytes tend to organise themselves into 3-dimensional hepatic cords and this organisation of the cells is the product of joint interaction between mature hepatocytes, nonparenchymal cells and the extra-cellular matrix[69]. On the other hand, the hepatocyte aggregates are simply constructed from mature hepatocytes alone and it is not possible to derive a true liver construct using these aggregates. Progenitor cells such as small hepatocytes (SH) cells[69, 83] have also been cultured in within 3-dimensional scaffolds to promote the formation of hepatic organoids. However, the sizes of the these aggregates confined within the pits of these 3-dimensional scaffold are limited by pits dimension[83]. As such, it had been rather difficult to reconstruct a well-assembled tissue in the scaffold as the assembly of cells into tissues is a highly complex process directed spontaneously by several types of cell. Yet, the precise organisation of the hepatocytes is essential in developing a viable bioartificial liver.

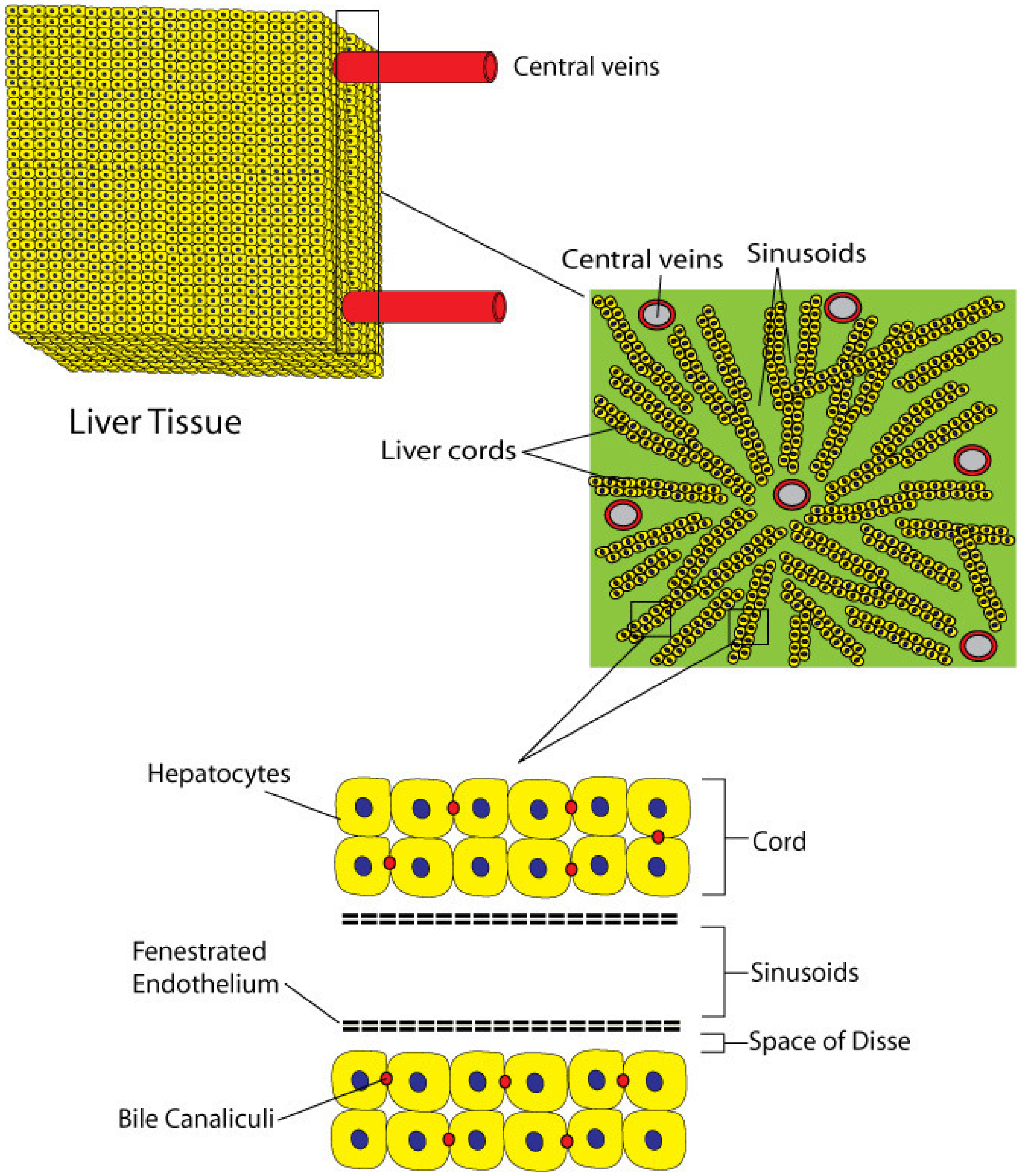

Figure 3.13 – Schematic view of the organisation of cells within the liver tissue. The organisation and formation of hepatocyte cords is a product of the joint interaction between many cell types.

In the previous section, we have demonstrated the cell culture on PEG functionalised pSi patterned with the laser microdissection microscope. pSi has already been demonstrated as a viable platform for maintaining long term hepatic functions in vitro[15, 86]. We hypothesised that by using the same ablation setup, it is possible to confine hepatocytes inside deep ablation trenches and to force them to stack on top of each other. Stacking of hepatocytes has been shown in the past as the precursors towards formation of liver organoids[87]. Furthermore, with the stacking of hepatocytes on deep trench, it is possible to realise an artificial hepatocyte cord without the usual need for the association with other cell types. In this section, we intend to artificially construct a hepatocyte cord on laser ablated micropatterned pSi and perform a preliminary study on the stacking formation within the trench. The schematic for the proposed experiment is as shown in figure 3.14. One advantage of using pSi is that its porous architecture can permit nutrients and biomolecules to diffuse throughout the layer. This might aid in maintaining the viability of the hepatocytes residing within the trench. Another excellent feature conferred by this laser ablation is the ability to designate the direction and the depth of these cords prior to cell seeding on the surface. This simple organisation of hepatocytes into cords by topographical confinement on the surface can contribute greatly towards the development of a bioartificial liver.

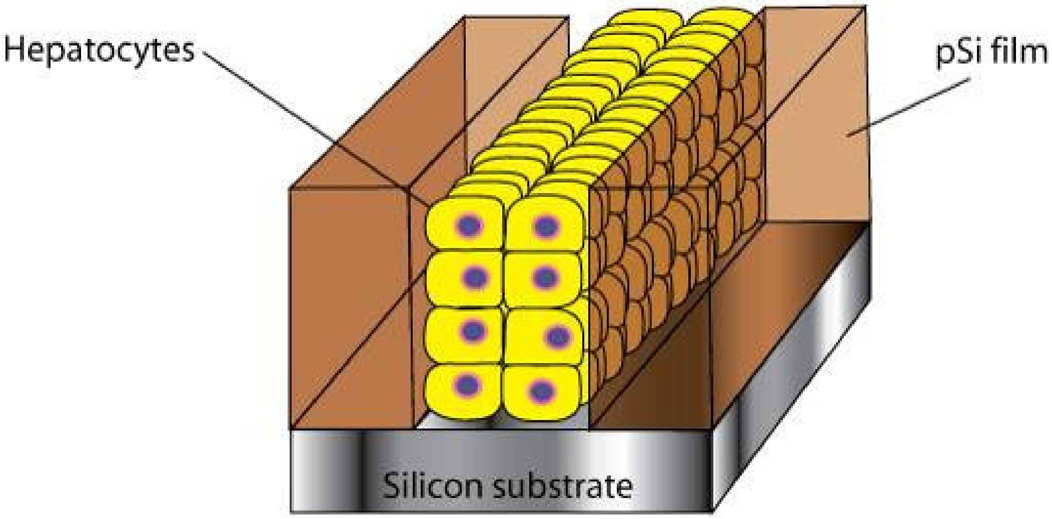

Figure 3.14 – 3D view of the hepatocyte cord within the ablated trench. The flow of bioactive molecules and nutrient is permitted by the porous architecture of the pSi film, thus further enhancing cell viability.

3.3.1 Methods and materials

pSi samples were prepared from p-type (boron-doped) silicon wafers with (100) orientation and resistivity of 0.0005-0.001 Ω·cm (Virginia Semiconductors). Samples were etched in a 3:1 (v/v) solution of 49% aqueous HF/EtOH for 300 and 600 seconds respectively at a constant current density of 133 mA/cm^2. After etching, the samples were rinsed with methanol, acetone and dichloromethane and were dried under a stream of N_2. The freshly etched pSi surfaces were oxidised by exposure to ozone at a flux of 8g/hr for 20 mins and subsequently rinsed with CH_2Cl_2 and EtOH.

3.3.1.1 Microdissection laser ablation

After the pSi surfaces were functionalised with PEG silane (See section 3.1.2), the surfaces were extensively washed with EtOH and dried with N_2 in a laminar flow hood. The pSi surfaces were subsequently ablated with a laser microdissection microscope (the power intensity for the laser was set at 40 and the transverse speed for the ablation was estimated to be at 30-40 μm per second). A 10x objective lens was used for all surface ablation. All lines were ablated from these two surfaces to only remove the pSi film while leaving the base silicon intact by the observation of the colour of the plume generated during ablation. For the pSi film etched for 300s, ablation was usually complete after 7-8 ablation repetitions were usually required while the film etched for 600s would generally require 14-15 repetitions.

3.2.1.2 Cell culture

Micropatterned pSi surfaces were first were rinsed with 95% EtOH and subsequently dried at room temperature in the laminar air flow. These surfaces were then aseptically transferred into sterile 6-well plates. A cell suspension H4IIE hepatoma cells at a density of 6.5 x 10^5 was seeded onto the surface. The surfaces were incubated at 37°C for 24 hours in filter sterilised Dulbecco's modified Eagle Medium (DMEM) that contains 10% (vol/vol) fetal bovine serum (FBS), 50 IU/ml penicillin and 50 mg/ml Streptomycin Sulphate and the pH was adjusted to 7.2 with 0.1M HCl.

3.2.1.3 SEM analysis

SEM was performed to observe the visual appearances of the ablated trenchs on the pSi surface. After incubation, the pSi surfaces were carefully removed from the 6-well plate, rinsed once with PBS and fixed in 3.7% formaldehyde in PBS for 10 mins at room temperature. Subsequently, the surfaces were washed again twice in PBS and incubated in turn in 50%, 75% and 100% EtOH for 10 mins. The surfaces were then washed twice in PBS, incubated in hexane, dried in the laminar airflow, and subsequently coated with platinum. Scanning electron microscopy (SEM) was performed on a Phillips XL30 field emission scanning electron microscope with an acceleration voltage of 10 kV.

3.2.1.4 Laser scanning confocal microscopy (LSCM)

At the end of the incubation time, the cells were incubated with 2 µg/ml of Hoechst 33342 dye for 30 mins before gently rinsing the wells twice with PBS. The cells were subsequently fixed with 3.7% formaldehyde in PBS for 10 mins at room temperature and washed with PBS. After fixation, 5mls of 0.1% Triton X-100 in PBS was added to each well for 5 mins and each well was rinsed again with PBS. 5 µl of 6.6 µM of Alexa Fluor® 594 phalloidin (Invitrogen) was added to 200 µl of PBS and the solution was added into each well and incubated in the dark for 30 mins. The cells were finally rinsed with PBS and stored in 10 % glycerol in PBS adjusted to pH 8.0 (buffered glycerol) in the dark. Confocal microscopy was performed on a Leica TCS SP5 laser scanning confocal microscope.

3.3.2 Results and discussion

3.3.2.1 Deep trench ablation with microdissection laser

To determine the influence of the depth of the trench on the formation of the hepatocytes cord, we had decided to produce two pSi films with different thickness. As ablation was performed to solely remove the porous layer while leaving the bulk silicon intact, the depth of the trench is therefore equivalent to the thickness of the film. This difference in film thickness was attained by changing the anodisation time for each of the films. The different anodisation times employed for these two separate films were 300 and 600 seconds, respectively. Since the film thickness is dependent on the time of anodisation, the thickness of the film doubles between 300 to 600 seconds.

To further narrow the width of the lines, the aperture setting was reduced. Ablation was performed on these thick films to only remove the porous layer while avoiding further ablation into the silicon substrate. This process was monitored by visually observing the colour of the plume formed on the microscope. As mentioned in the previous section, we noticed that when the ablation was performed solely on pSi film, the colour of the plume formed was orange while the ablation on bare silicon would yield a bluish white plume. Due to the difference in anodisation time for the 2 films the ablation cycles to completely ablate the porous layers were different. To completely ablate a line on a pSi film etched for 300s, 7-8 ablation runs on the same line were usually required for the film while films etched for 600s would generally require 14-15 cycles.

After the ablation and functionalisation, H4IIE hepatoma cells were seeded on the surface for 24 hours incubation. Following that, we cells were fixed [34, 88] for SEM imaging in an attempt to observe the hepatocyte cords growing inside the ablated trenches. Unfortunately, the hepatocyte cords were unable to withstand the harsh fixation procedure and these cords had mostly dislodged from the trench during the procedure. Still, we were able to observe a few cells residing within some of the ablated trenches by SEM as shown in figure 3.15.

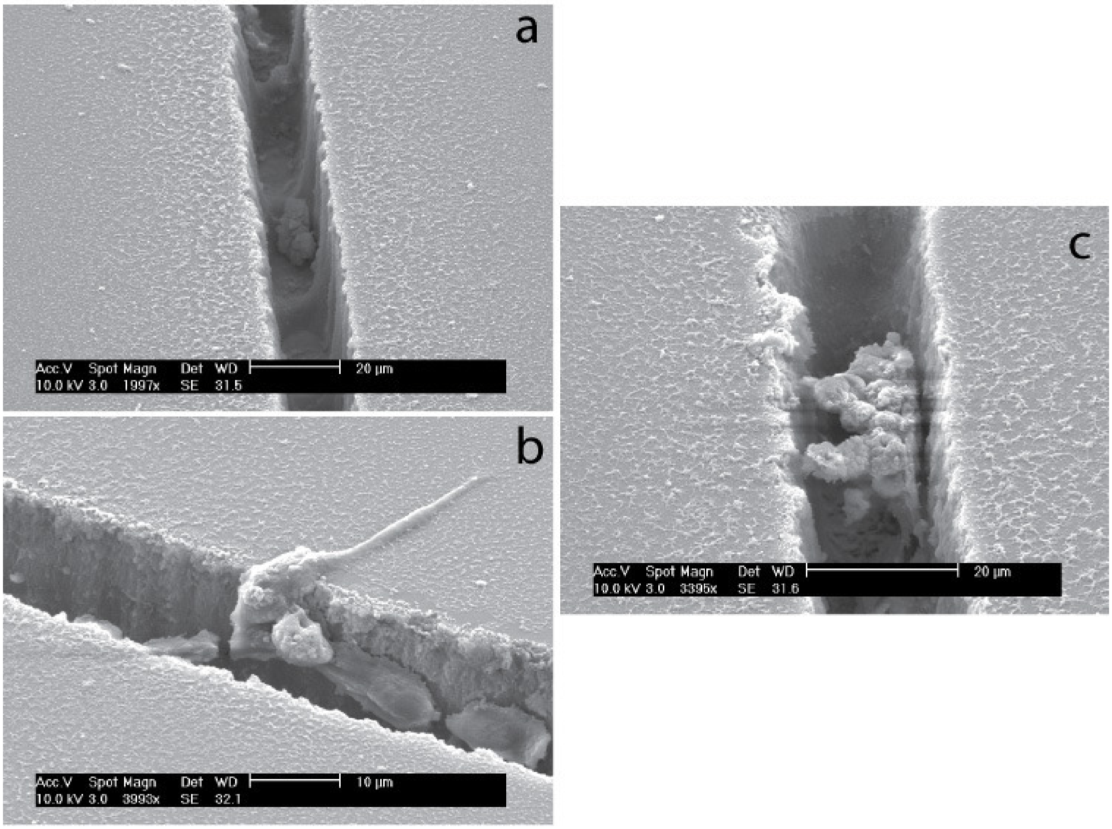

Figure 3.15 – SEM micrograph of hepatocyte cells residing in deeply ablated trench (aperture setting 40) on the thickest pSi film (etched for 600s). (a) Deeply ablated trench on the pSi surface. Note some cells attaching at the bottom of the trench. (b) Cellular projections protruding out from the trench and attaching to the pSi surface. (c) The shriveled appearance of a cellular cluster within the trench (anodized for 300s) is attributed to the fixation procedure.

SEM imaging on trenches ablated on the thickest pSi film revealed that the deep trenches had an average width of 20 µm. The trenches were slightly narrower compared to those produced in the previous section since the aperture was reduced in order to further reduce the width of the laser beam. Due to the brittleness of the thick pSi film, it tended to shatter and break into smaller fragments upon scoring with a diamond cutter on the surface. Therefore, we were unable to accurately measure the actual depth of these trenches. Interestingly, for some of the trenches with cells that remained after the fixation process, we observed cellular attachments along the side walls of these trenches (figure 3.15 (c)). This strongly suggested that apart from the intercellular support conferred from the underlying multilayered cell stacks, cells was able to rely on attachment to the side walls in the trenches to strengthen their attachment on the surface. In general, SEM images showed that these trenches were sufficiently deep for the formation of 2-4 cells multilayered stack to form the hepatocyte cords.

3.3.2.2 Confocal microscopy analysis

Laser scanning confocal microscopy was employed to investigate the formation of cell stacking inside the lines ablated on the two different pSi films. Since ablation was performed only to exclusively remove the porous film, the ablation depth was thus dependent on the film thickness. After 24 hours incubation of the H4IIE hepatoma cells on the two different films, the cell nuclei were stained with Hoechst dye, while the cytoskeletal F-actin network was stained with phalloidin tagged with an Alexa Fluor® fluorophore.

Figure 3.16 shows confocal microscopy images of the hepatocytes growing on one ablated line for the pSi film etched for 300s. When imaging the trench along the x-z axis, we noticed that due to effects of luminescence displayed by the pSi film between 12-18 µm into the z plane, it was possible to visually resolve the outline of the trench. The luminescence effect of the pSi film is as shown in figure 3.16 (a) and the hepatocyte cells were found to be well-confined within the trench. By tilting the confocal images taken along the x-z axis, we noticed that cells on these trenches did not form a layer on the same plane and the position of the individual nuclei had confirmed that the hepatocytes had indeed formed a multilayered stack (figure 3.16 (b)). This indicates that cells inside deeper trenches were able to form multilayer cell stacks that closely resembles the morphology of typical hepatocyte cords[69, 89].

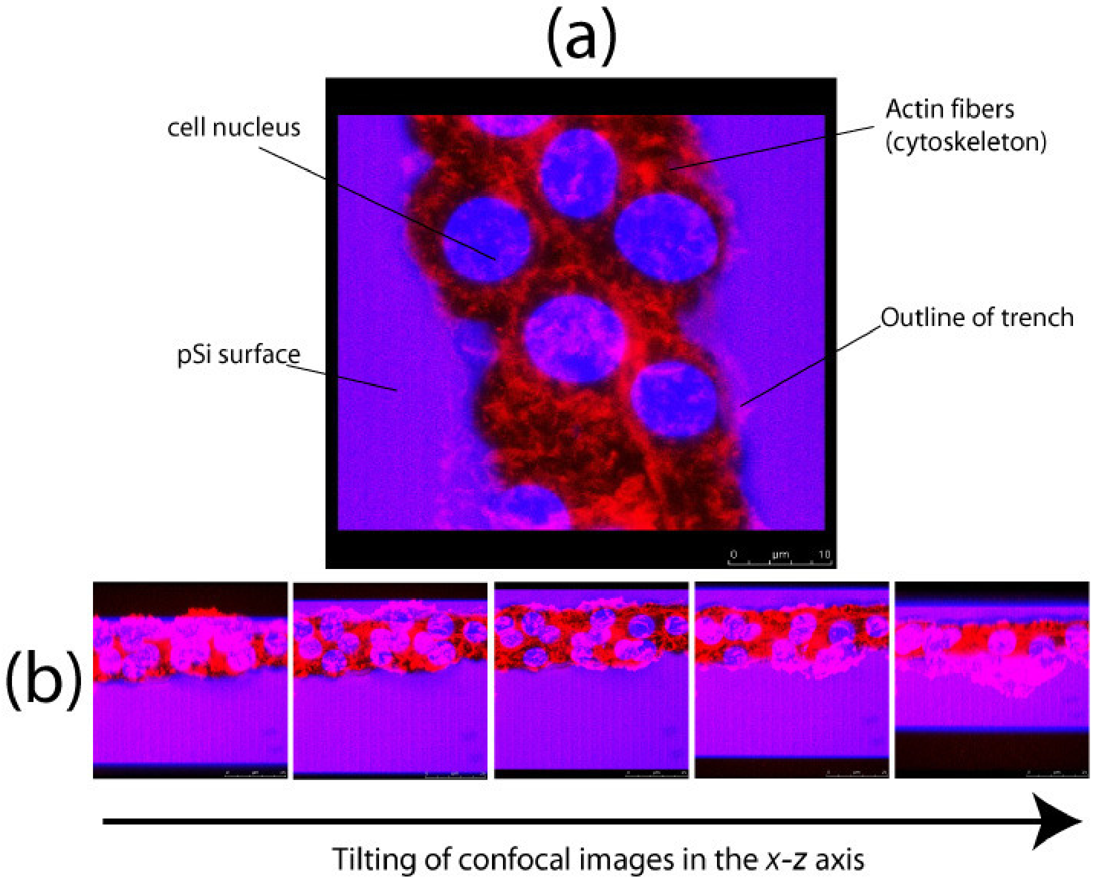

Figure 3.16 – (a) Laser scanning confocal image of hepatocytes stained with Hoechst 33342 and Alexa Fluor® phalloidin conjugate after 24 hours of growth on ablated lines on films etched for 300s. Cells were well confined within the trench and (b) 3-dimensional volume image derived from a series of tilting had confirm the presence of two cell layers

To further characterise and confirm the multilayered stacking for the trench ablated on the pSi film etched for 300s, the confocal microscopy images were 3-dimensionally reconstructed for cells residing on these trenches. This 3-dimensional reconstruction of the trench was achieved by calculating 35 planes at 0.7 µm intervals (figure 3.17). The 1st and the 35th plane were taken at the both extreme ends from the top and the bottom of the trench and the distance was measured at 24.6 µm. Since ablation was performed to completely remove the porous layer from the silicon substrate, the depth of trench is approximately the thickness of the porous layer and thus the depth is approximately 24.6 µm.

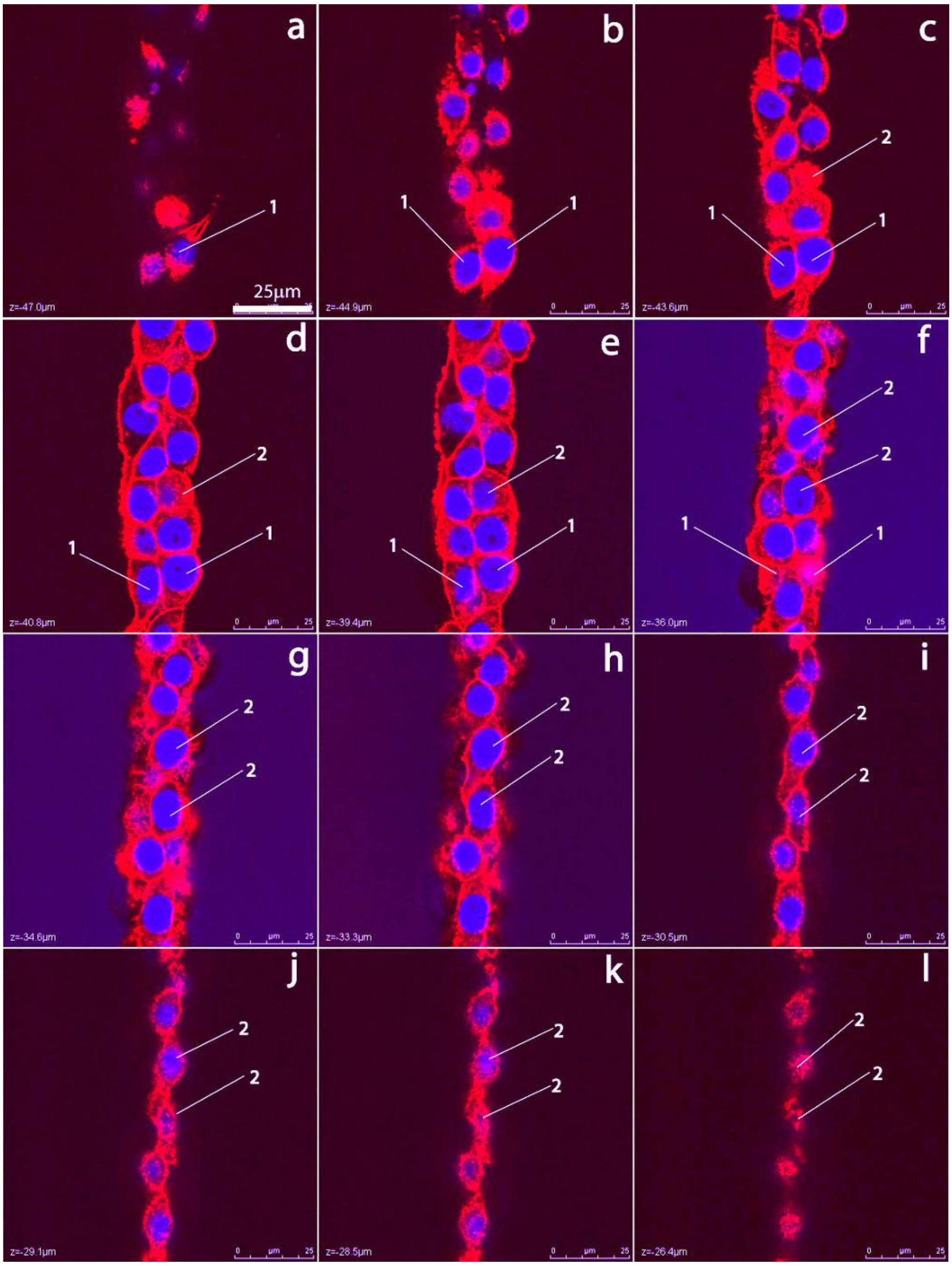

Figure 3.17 – Laser scanning confocal images taken at different z planes (z stack) showing a trench ablated on pSi film etched for 300s in 0.7 µm intervals; (a) 2.1 µm, (b) 4.2 µm, (c) 5.6 µm (d) 8.4 µm, (e) 9.8 µm, (f) 13.3 µm, (g) 14.7 µm, (h) 16.1 µm, (i) 18.9 µm, (j) 20.3 µm, (k) 21 µm and (l) 23.1 µm from the top of the pSi surface into the bottom of the trench. Numbers as denoted represents the cell layer, (1) top layer and (2) bottom layer. Note that the luminescence effect of pSi was only observable between 12-18 µm into the z planes.

As the plane of view proceeds deeper into the trench (figure 3.17 (a)-(f)), cell nuclei from the top layer (denoted as number 1) gradually disappear while cell nuclei from the second bottom layer (denoted as number 2) appear. Image analysis gave a thickness of 11.2 µm for the top cell layer. As this was measured on a stacked cell that were not fully spread, this value do compared favorably to the average diameter (14 µm) reported in literature for a fully spreaded H4IIE cell on a flat surface[90]. Subsequently, as the plane of view proceeds further (figure 3.17 (g)-(l)), it was no longer possible to observe cell nuclei from the top layer. The thickness of the second cell layer was measured at 9.8 µm, once again matching the diameter of the hepatocyte. One important observation was that while the top layer had an average width of 2 cells, the bottom layer was made of a single file of cells. This was attributed to the fact that the ablation on the surface did not produce a trench with straight walls and a square profile, but rather a conical one, narrowing towards the bottom of the trench. Whilst we were unable to image the cross-section of the trench by SEM, images taken from top view of the trench (figure 3.15) appeared to narrow towards the base. So the sterics of the trench appear to only allow the attachment of a single cell column at the base of the trench.

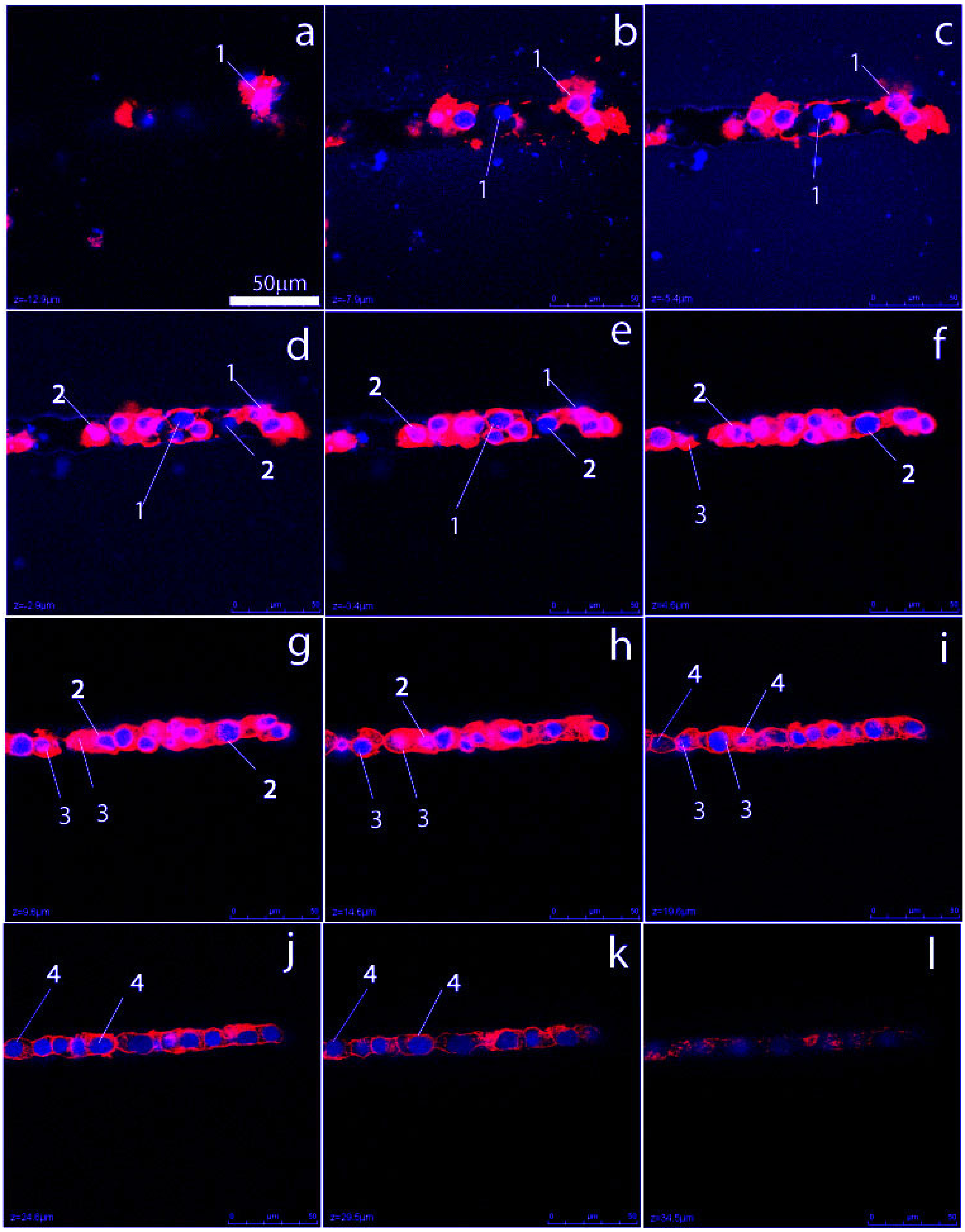

Figure 3.18 – 3-dimensional deconvolution of a trench ablated on a pSi film etched for 600s, reconstructing from 20 planes at 2.5 µm intervals; (a) 5 µm, (b) 10 µm, (c) 12.5 µm, (d) 15 µm, (e) 17.5 µm, (f) 20 µm, (g) 25 µm, (h) 30 µm, (i) 3.5 µm, (j) 40 µm, (k) 45 µm and (l) 50 µm from the top of the pSi surface into the bottom of the trench. Numbers as denoted represents the cell layer, (1) first layer, (2) second layer (3) third layer and (4) fourth layer.

Based on the above observation, we could expected a higher level of cell stacking for trenches ablated on the thicker pSi film that was etched for 600s. 3-dimensional reconstruction of the cell stack in one of these deeper trenches was calculated from 20 planes at 2.5 µm intervals (figure 3.18). Results had indeed shown a higher cell stacking within these deeper trenches. As the plane of view proceeds into the trench (figure 3.18 (a)-(e)), resolution of cell nucleus from the first layer (denoted as number 1) gradually disappeared while cell nucleus from the second layer (denoted as number 2) gained contrast. Subsequently, cell nuclei from second cell layer also disappeared as the plane of view moved deeper, as shown in figure 3.18 (e)-(f). The third layer of cell nucleus can be observed appearing between the 10th and the 14th interval (figure 3.18 (g)-(i)). Subsequently, as the plane of view proceeds deeper into the trench (figure 3.18 (i)-(l)), the fourth layer of cells nuclei was finally revealed. Once again, the attachment of a single cell column at the base of the trench had confirmed the narrowing of the trench towards the base.

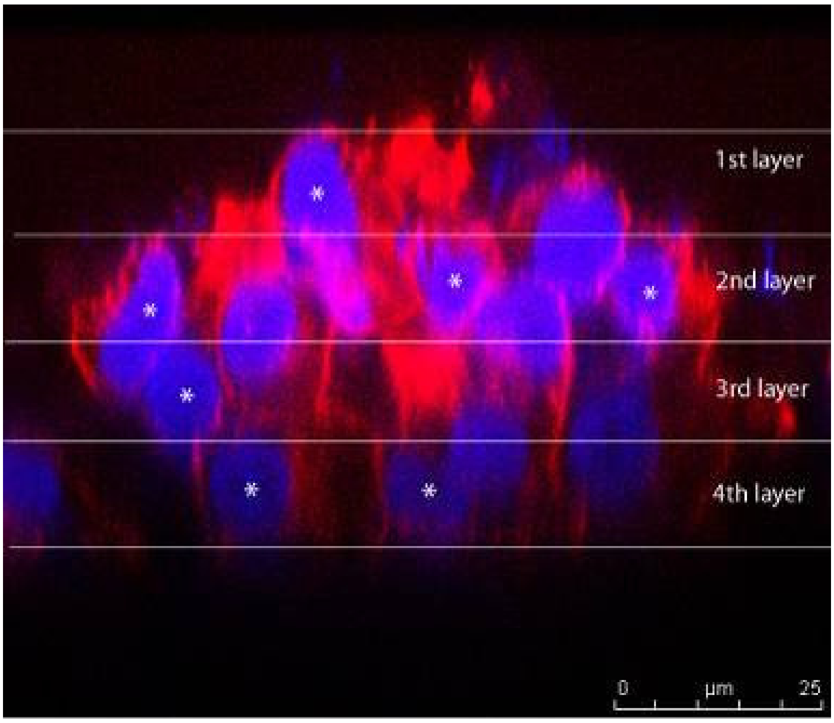

Figure 3.19 – An x-z image reconstruction of the cell multilayer in the stack. The horizontal axis is the direction of the trench, whilst the vertical axis is the surface normal. Asterisks indicate the positions of the cell nuclei that correspond to the each of individual layers. The white horizontal lines are as a guide to the eye only.

The formation of a 4 cell layer stack was further confirmed by 3-dimensional reconstruction along the x-z axis of the trench. From figure 3.19, a 4 cell layer stack could be determined in the x-z image with positions of the cell nuclei corresponding to the layer as denoted by the asterisks. The layers were found to be rather disordered. A few interesting conclusions can be drawn from the deeper trench ablated on the films etched for 600s. Firstly, from the image in Figure 3.19, the distance from the top of the cell stack to the bottom was measured at approximately 50 µm. This distance was double of that measured for the pSi film etched for 300s and this was expected as the anodisation time was exactly doubled. Secondly, with the doubling of the film thickness, the cell layers had also increased from a 2 cell stack to a 4 cell stack. The narrowing at the base of the trench was also evidenced by appearance of single cell column at the bottom of the trench while cells closer to the top were able to form 2 cell columns.

From a series of different x-z scans, we had determined that the average number of hepatocyte cells that can be confined within a 1 mm long ablated trench is approximately 69 for the film etched for 300s and 181 cells for the films etched for 600s. More importantly, we have also confirmed that H4IIE hepatoma cells stacked inside the ablated trench had displayed cell morphology compatible to the hepatocyte cord found *in vivo* by a comparison to previous research in literature. For the long term maintenance of hepatocytes *in vitro,* co-cultures sandwiches were often used[69, 70, 72]. Previously, Sudo et.al[69] had reported using the sandwich setup to produce viable hepatocyte cords. In this setup, hepatocytes were sandwiched between layers of porous membrane that mimic the fenestrated endothelium. This closely resembles the environment found in the natural liver and an extended maintenance of bile function for more than 20 days was achieved. Confocal imaging of the stacked hepatocytes (figure 3.20 (a)) had revealed the hepatocyte stack was growing confluently on the cultured surface.

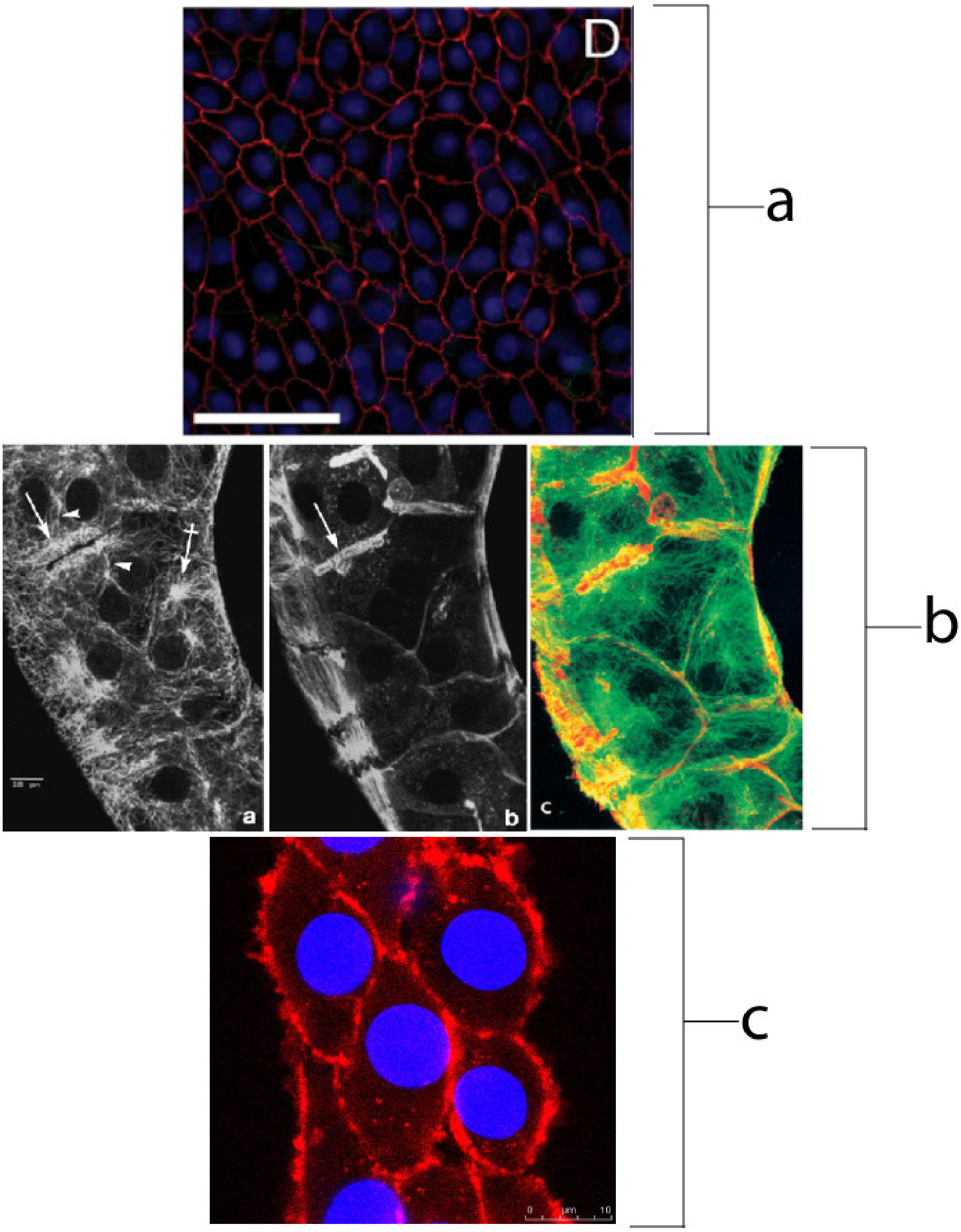

Figure 3.20– A comparison for the formation hepatocyte cords reported in literature. (a) The assembly of hepatocyte cord *in vitro* reported Sudo et.al[69] that uses an unique cell stacking arrangement that closely mimic the cellular setup *in vivo.* (b) Hepatocyte cords isolated from rat liver and stained from actin and microtubules as reported by Novikoff et.al[89]. (c) An example from confocal imaging of our existing work using ablated pSi trench.

Although the sandwich stacking of the hepatocytes on such a system does closely mimic actual conditions in the liver, these systems do not fully represent actual hepatocyte cord due to the lack of the sinusoid spacing that is normally found between hepatocyte cords *in vivo*. An isolate from fresh liver tissue had shown that hepatocyte cords are generally a couple of cells wide and normally divided by a sinusoidal space, as reported in the work by Novikoff[89] and is as shown in figure 3.20 (b). It is also interesting to note that individual hepatocyte in the cords have a rounder cell morphology due to presence of radiating actin fiber diverging from the loci of the cell as observed by Novikoff et.al[89]. Cells cultured on surfaces *in vitro* had a more ovalish morphology due to being more densely packed layer, as shown in figure 3.20 (a). Confocal images of hepatocyte in our work, as shown in figure 3.20 (c), also displayed such ovalish morphology when residing inside these trenches. However, it is obvious from the visual comparison that our strategy of using trenches to confine hepatocyte cells bears closer structural resemblance to that of the actual cord. Thus, by means of spatial confinement, we have demonstrated that it is possible to assembly a structurally resembling hepatocyte cord without sandwich systems and walls

3.3.3 Conclusions

Deep laser ablation of a pSi film has been utilized for the reconstruction of artificial hepatocyte cords. Hepatocytes multilayers after 24 hours cell culture and cell attachment was restricted to the ablated regions. The observation of the colour of the plume generated by laser ablation is a good indicator to the extent of the ablation on the surface.

Although the depth of the trench could not be determined by SEM, confocal imaging enabled us to reveal the depth in which the cells were residing inside these trenches. As such, we found that by ablating away the porous layer of a pSi film to produce a trench approximately 25 µm depth, we can produce a 2-layer hepatocyte stack. By doubling the depth of the trench to 50 µm, we can produce a 4-layer hepatocyte stack. The hepatocyte stacks imaged under the confocal microscopy showed good structural symmetry to natural cords as reported in literature[89]

In brief, we have shown that laser ablation of pSi films allows the formation of hepatocyte multilayers. This is the first step in reconstructing complex 3-dimensional liver structures. This approach is an alternative to conventional spheroid-based liver cell culture. The viability and metabolism of these structures were not investigated in this work and will certainly be a focus for future studies.

REFERENCES

1. Park, T. H.; Shuler, M. L., Integration of cell culture and microfabrication technology. *Biotechnology Progress* 2003, 19, (2), 243-253.

2. Ziauddin, J.; Sabatini, D. M., Microarrays of cells expressing defined cDNAs. *Nature* 2001, 411, (6833), 107-110.

3. Folch, A.; Toner, M., Microengineering of cellular interactions. *Annual Review of Biomedical Engineering* 2000, 2, 227-256.

4. Saltzman, W. M.; Olbricht, W. L., Building drug delivery into tissue engineering. *Nature Reviews Drug Discovery* 2002, 1, (3), 177-186.

5. Recknor, J. B.; Recknor, J. C.; Sakaguchi, D. S.; Mallapragada, S. K., Oriented astroglial cell growth on micropatterned polystyrene substrates. *Biomaterials* 2004, 25, (14), 2753-2767.

6. Chang, J. C.; Brewer, G. J.; Wheeler, B. C., A modified microstamping technique enhances polylysine transfer and neuronal cell patterning. *Biomaterials* 2003, 24, (17), 2863-2870.

7. Xia, Y.; Whitesides, G. M., Soft lithography. *Angewandte Chemie, International Edition* 1998, 37, (5), 550-575.

8. Lee, K.-B.; Park, S.-J.; Mirkin, C. A.; Smith, J. C.; Mrksich, M., Protein nanoarrays generated by dip-pen nanolithography. *Science (Washington, DC, United States)* 2002, 295, (5560), 1702-1705.

9. Gallant, N. D.; Michael, K. E.; Garcia, A. J., Cell adhesion strengthening: Contributions of adhesive area, integrin binding, and focal adhesion assembly. *Molecular Biology of the Cell* 2005, 16, (9), 4329-4340.

10. Pan, Y. V.; McDevitt, T. C.; Kim, T. K.; Leach-Scampavia, D.; Stayton, P. S.; Denton, D. D.; Ratner, B. D., Micro-Scale Cell Patterning on Nonfouling Plasma Polymerized Tetraglyme Coatings by Protein Microcontact Printing. *Plasmas and Polymers* 2002, 7, (2), 171-183.

11. Takayama, S.; McDonald, J. C.; Ostuni, E.; Liang, M. N.; Kenis, P. J. A.; Ismagilov, R. F.; Whitesides, G. M., Patterning cells and their environments using multiple laminar fluid flows in capillary networks. *Proceedings of the National Academy of Sciences of the United States of America* 1999, 96, (10), 5545-5548.

12. Szili, E.; Thissen, H.; Hayes, J. P.; Voelcker, N., A biochip platform for cell transfection assays. *Biosensors & Bioelectronics* 2004, 19, (11), 1395-1400.

13. **Thissen, H.; Hayes, J. P.; Kingshott, P.; Johnson, G.; Harvey, E. C.; Griesser, H. J., Nanometer thickness laser ablation for spatial control of cell attachment.** ***Smart Materials and Structures*** **2002, 11, (5), 792-799.**

14. **Canham, L. T., Bioactive silicon structure fabrication through nanoetching techniques.** ***Advanced Materials (Weinheim, Germany)*** **1995, 7, (12), 1033-7.**

15. **Chin, V.; Collins, B. E.; Sailor, M. J.; Bhatia, S. N., Compatibility of primary hepatocytes with oxidized nanoporous silicon.** ***Advanced Materials*** **2001, 13, (24), 1877-+.**

16. **Sapelkin, A. V.; Bayliss, S. C.; Unal, B.; Charalambou, A., Interaction of B50 rat hippocampal cells with stain-etched porous silicon.** ***Biomaterials*** **2006, 27, (6), 842-846.**

17. **Janshoff, A.; Dancil, K. P. S.; Steinem, C.; Greiner, D. P.; Lin, V. S. Y.; Gurtner, C.; Motesharei, K.; Sailor, M. J.; Ghadiri, M. R., Macroporous p-type silicon Fabry-Perot layers. Fabrication, characterization, and applications in biosensing.** ***Journal Of The American Chemical Society*** **1998, 120, (46), 12108-12116.**

18. **Tinsley-Bown, A. M.; Canham, L. T.; Hollings, M.; Anderson, M. H.; Reeves, C. L.; Cox, T. I.; Nicklin, S.; Squirrell, D. J.; Perkins, E.; Hutchinson, A.; Sailor, M. J.; Wun, A., Tuning the pore size and surface chemistry of porous silicon for immunoassays.** ***Physica Status Solidi A: Applied Research*** **2000, 182, (1), 547-553.**

19. **Stewart, M. P.; Buriak, J. M., Chemical and biological applications of porous silicon technology.** ***Advanced Materials (Weinheim, Germany)*** **2000, 12, (12), 859-869.**

20. **Bayliss, S. C.; Buckberry, L. D.; Fletcher, I.; Tobin, M. J., The culture of neurons on silicon.** ***Sensors and Actuators, A: Physical*** **1999, A74, (1-3), 139-142.**

21. **Bayliss, S. C.; Buckberry, L. D.; Harris, P. J.; Tobin, M., Nature of the silicon-animal cell interface.** ***Journal of Porous Materials*** **2000, 7, (1/2/3), 191-195.**

22. **Bayliss, S. C.; Heald, R.; Fletcher, D. I.; Buckberry, L. D., The culture of mammalian cells on nanostructured silicon.** ***Advanced Materials (Weinheim, Germany)*** **1999, 11, (4), 318-321.**

23. **Dorvee, J. R.; Derfus, A. M.; Bhatia, S. N.; Sailor, M. J., Manipulation of liquid droplets using amphiphilic, magnetic one-dimensional photonic crystal chaperones.** ***Nature Materials*** **2004, 3, (12), 896-899.**

24. **Lin, V. S. Y.; Motesharei, K.; Dancil, K.-P. S.; Sailor, M. J.; Ghadiri, M. R., A porous silicon-based optical interferometric biosensor.** ***Science (Washington, D. C.)*** **1997, 278, (5339), 840-843.**

25. **Steinem, C.; Janshoff, A.; Lin, V. S. Y.; Voelcker, N. H.; Reza Ghadiri, M., DNA hybridization-enhanced porous silicon corrosion: mechanistic investigations and prospect for optical interferometric biosensing.** ***Tetrahedron*** **2004, 60, (49), 11259-11267.**

26. Anglin, E. J.; Schwartz, M. P.; Ng, V. P.; Perelman, L. A.; Sailor, M. J., Engineering the chemistry and nanostructure of porous Silicon Fabry-Perot films for loading and release of a steroid. ***Langmuir*** **2004, 20, (25), 11264-11269.**

27. Liu Tsang, V.; Bhatia, S. N., Three-dimensional tissue fabrication. ***Advanced Drug Delivery Reviews*** **2004, 56, (11), 1635-1647.**

28. Ji, J.; Li, X.; Canham, L. T.; Coffer, J. L., Use of microcontact printing methods to direct pattern formation of calcified mesoporous silicon. ***Advanced Materials (Weinheim, Germany)*** **2002, 14, (1), 41-43.**

29. Sirbuly, D. J.; Lowman, G. M.; Scott, B.; Stucky, G. D.; Buratto, S. K., Patterned microstructures of porous silicon by dry-removal soft lithography. ***Advanced Materials (Weinheim, Germany)*** **2003, 15, (2), 149-152.**

30. Kabashin, A. V.; Meunier, M., Fabrication of photoluminescent Si-based layers by air optical breakdown near the silicon surface. ***Applied Surface Science*** **2002, 186, (1-4), 578-582.**

31. Savin, D. P.; Roizin, Y. O.; Demchenko, D. A.; Mugenski, E.; Sokoiska, I., Properties of laser ablated porous silicon. ***Applied Physics Letters*** **1996, 69, (20), 3048-3050.**

32. Hashimoto, A.; Iwata, K.; Ohkubo, M.; Yamamoto, A., New laser ablation phenomenon of the porous Si films by focused N2 pulse laser irradiation. ***Journal of Applied Physics*** **1994, 75, (10, Pt. 1), 5447-9.**

33. Rossi, A. M.; Borini, S.; Boarino, L.; Amato, G., Lateral structuring of porous silicon: Application to waveguides. ***Physica Status Solidi A: Applied Research*** **2003, 197, (1), 284-287.**

34. Khung, Y. L.; Barritt, G.; Voelcker, N. H., Using continuous porous silicon gradients to study the influence of surface topography on the behaviour of neuroblastoma cells. ***Experimental Cell Research*** **2008, 314, 789-800.**

35. Gao, T.; Gao, J.; Sailor, M. J., Tuning the response and stability of thin film mesoporous silicon vapor sensors by surface modification. ***Langmuir*** **2002, 18, (25), 9953-9957.**

36. Xu, D.; Sun, L.; Li, H.; Zhang, L.; Guo, G.; Zhao, X.; Gui, L., Hydrolysis and silanization of the hydrosilicon surface of freshly prepared porous silicon by an amine catalytic reaction. ***New Journal of Chemistry*** **2003, 27, (2), 300-306.**

37. Thomas, J. J.; Shen, Z.; Crowell, J. E.; Finn, M. G.; Siuzdak, G., Desorption/ionization on silicon (DIOS): a diverse mass spectrometry platform for protein characterization. ***Proceedings of the National Academy of Sciences of the United States of America*** **2001, 98, (9), 4932-4937.**

38. Wei, J.; Buriak, J. M.; Siuzdak, G., Desorption-ionization mass spectrometry on porous silicon. ***Nature (London)*** **1999, 399, (6733), 243-246.**

39. Canham, L.; Editor, *Properties of Porous Silicon. [In: EMIS Datarev. Ser., 1997; 18]*. 1997; p 405 pp.
40. Kan, P. Y. Y.; Finstad, T. G., Oxidation of macroporous silicon for thick thermal insulation. *Materials Science and Engineering B-Solid State Materials for Advanced Technology* 2005, 118, (1-3), 289-292.

41. Matsuzawa, M.; Krauthamer, V.; Potember, R. S., Directional guidance of neurite outgrowth using substrates patterned with biomaterials. *Biosystems* 1995, 35, (2-3), 199-202.

42. Matsuzawa, M.; Potember, R. S.; Stenger, D. A.; Krauthamer, V., Containment and growth of neuroblastoma cells on chemically patterned substrates. *Journal of neuroscience methods* 1993, 50, (2), 253-60.

43. Cos, S.; Verduga, R.; Fernandez-Viadero, C.; Megias, M.; Crespo, D., Effects of melatonin on the proliferation and differentiation of human neuroblastoma cells in culture. *Neuroscience Letters* 1996, 216, (2), 113-116.

44. Zagon, I. S.; McLaughlin, P. J., Opioids and differentiation in human cancer cells. *Neuropeptides (Amsterdam, Netherlands)* 2005, 39, (5), 495-505.

45. Ben, L.-H.; Zhao, J.; Xin, S.-M.; Luo, S.-Q.; Pei, G., Attenuation of d opioid receptor-mediated signaling by kainic acid in neural cells: involvement of protein kinase C and intracellular Ca2+. *Neuropharmacology* 1999, 38, (7), 991-998.

46. Los, G. V.; Artemenko, I. P.; Hokin, L. E., Time-dependent effects of lithium on the agonist-stimulated accumulation of second messenger inositol 1,4,5-trisphosphate in SH-SY5Y human neuroblastoma cells. *Biochemical Journal* 1995, 311, (1), 225-32.

47. Moolwaney, A. S.; Igwe, O. J., Regulation of the cyclooxygenase-2 system by interleukin-1b through mitogen-activated protein kinase signaling pathways: A comparative study of human neuroglioma and neuroblastoma cells. *Molecular Brain Research* 2005, 137, (1-2), 202-212.

48. Barnes, E. N.; Biedler, J. L.; Spengler, B. A.; Lyser, K. M., The fine structure of continuous human neuroblastoma lines SK-N-SH, SK-N-BE(2), and SK-N-MC. *In vitro* 1981, 17, (7), 619-31.

49. Schlesinger, H. R.; Gerson, J. M.; Moorhead, P. S.; Maguire, H.; Hummeler, K., Establishment and characterization of human neuroblastoma cell lines. *Cancer Research* 1976, 36, (9, Pt. 1), 3094-100.

50. Guillaume-Gentil, O.; Akiyama, Y.; Schuler, M.; Tang, C.; Textor, M.; Yamato, M.; Okano, T.; Voros, J., Polyelectrolyte coatings with a potential for electronic control and cell sheet engineering. *Advanced Materials* 2008, 20, (3), 560-+.

51. Matsuda, N.; Shimizu, T.; Yamato, M.; Okano, T., Tissue engineering based on cell sheet technology. *Advanced Materials* 2007, 19, (20), 3089-3099.

52. Ohashi, K.; Yokoyama, T.; Yamato, M.; Kuge, H.; Kanehiro, H.; Tsutsumi, M.; Amanuma, T.; Iwata, H.; Yang, J.; Okano, T.; Nakajima, Y., Engineering functional two- and three-dimensional liver systems in vivo using hepatic tissue sheets. *Nature Medicine* 2007, 13, (7), 880-885.

53. Fromherz, P., Electrical interfacing of nerve cells and semiconductor chips. *Chemphyschem* 2002, 3, (3), 276-284.

54. Fromherz, P., Three levels of neuroelectronic interfacing - Silicon chips with ion channels, nerve cells, and brain tissue. In *Progress in Convergence: Technologies for Human Wellbeing*, 2006; Vol. 1093, pp 143-160.

55. Sin, A.; Chin, K. C.; Jamil, M. F.; Kostov, Y.; Rao, G.; Shuler, M. L., The design and fabrication of three-chamber microscale cell culture analog devices with integrated dissolved oxygen sensors. *Biotechnology Progress* 2004, 20, (1), 338-345.

56. Nicolini, C.; Lanzi, M.; Accossato, P.; Fanigliulo, A.; Mattioli, F.; Martelli, A., A silicon-based biosensor for real-time toxicity testing in normal versus cancer liver-cells. *Biosensors & Bioelectronics* 1995, 10, (8), 723-733.

57. Khamsi, R., Labs on a chip: Meet the stripped down rat. *Nature* 2005, 435, (7038), 12-13.

58. Yeon, J. H.; Park, J. K., Cytotoxicity test based on electrochemical impedance measurement of HepG2 cultured in microfabricated cell chip. *Analytical Biochemistry* 2005, 341, (2), 308-315.

59. Wolbers, F.; ter Braak, P.; Le Gac, S.; Luttge, R.; Andersson, H.; Vermes, I.; van den Berg, A., Viability study of HL60 cells in contact with commonly used microchip materials. *Electrophoresis* 2006, 27, (24), 5073-5080.

60. de-Leon, S. B. T.; Oren, R.; Spira, M. E.; Korbakov, N.; Yitzchaik, S.; Sa'ar, A., Porous silicon substrates for neurons culturing and bio-photonic sensing. *Physica Status Solidi A-Applications And Materials Science* 2005, 202, (8), 1456-1461.

61. Martinoia, S.; Bove, M.; Tedesco, M.; Margesin, B.; Grattarola, M., A simple microfluidic system for patterning populations of neurons on silicon micromachined substrates. *Journal of neuroscience methods* 1999, 87, (1), 35-44.

62. Griscom, L.; Degenaar, P.; LePioufle, B.; Tamiya, E.; Fujita, H., Techniques for patterning and guidance of primary culture neurons on micro-electrode arrays. *Sensors And Actuators B-Chemical* 2002, 83, (1-3), 15-21.

63. Lee, J. W.; Lee, K. S.; Cho, N.; Ju, B. K.; Lee, K. B.; Lee, S. H., Topographical guidance of mouse neuronal cell onSiO(2) microtracks. *Sensors And Actuators B-Chemical* 2007, 128, (1), 252-257.

64. Specht, C. G.; Williams, O. A.; Jackman, R. B.; Schoepfer, R., Ordered growth of neurons on diamond (vol 25, pg 4073, 2004). *Biomaterials* 2005, 26, (7), 828-828.

65. Aleksandrovsky, A. S.; Potseluyko, A. M.; Seredkin, V. A.; Zaitsev, A. I.; Zamkov, A. V., Pulsed laser deposition and characterization of europium borate glass films. *Thin Solid Films* 2005, 483, (1-2), 27-30.

66. Tang, S. B.; Lai, M. O.; Lu, L., Effects of oxygen pressure on LiCoO2 thin film cathodes and their electrochemical properties grown by pulsed laser deposition. *Journal of Alloys and Compounds* 2006, 424, (1-2), 342-346.

67. Conde, J. C.; Lusquinos, F.; Gonzalez, P.; Serra, J.; Leon, B.; Cultrera, L.; Guido, D.; Perrone, A., Laser ablation of silicon and copper targets. Experimental and finite elements studies. *Applied Physics a-Materials Science & Processing* 2004, 79, (4-6), 1105-1110.

68. Miloso, M.; Villa, D.; Crimi, M.; Galbiati, S.; Donzelli, E.; Nicolini, G.; Tredici, G., Retinoic acid-induced neuritogenesis of human neuroblastoma SH-SY5Y cells is ERK independent and PKC dependent. *Journal of Neuroscience Research* 2003, 75, (2), 241-252.

69. Sudo, R.; Mitaka, T.; Ikeda, M.; Tanishita, K., Reconstruction of 3D stacked-up structures by rat small hepatocytes on microporous membranes. *FASEB Journal* 2005, 19, (10), 1695-+.

70. Du, Y.; Han, R. B.; Wen, F.; San, S. N. S.; Xia, L.; Wohland, T.; Leo, H. L.; Yu, H., Synthetic sandwich culture of 3D hepatocyte monolayer. *Biomaterials* 2008, 29, (3), 290-301.

71. Bokhari, M.; Carnachan, R. J.; Cameron, N. R.; Przyborski, S. A., Culture of HepG2 liver cells on three dimensional polystyrene scaffolds enhances cell structure and function during toxicological challenge. *Journal of Anatomy* 2007, 211, (4), 567-576.

72. Bi, Y. A.; Kazolias, D.; Duignan, D. B., Use of cryopreserved human hepatocytes in sandwich culture to measure hepatobiliary transport. *Drug Metabolism and Disposition* 2006, 34, (9), 1658-1665.

73. Mitaka, T., The current status of primary hepatocyte culture. *International Journal of Experimental Pathology* 1998, 79, (6), 393-409.

74. Nishikawa, Y.; Tokusashi, Y.; Kadohama, T.; Nishimori, H.; Ogawa, K., Hepatocytic cells form bile duct-like structures within a three-dimensional collagen gel matrix. *Experimental Cell Research* 1996, 223, (2), 357-371.

75. Koide, N.; Sakaguchi, K.; Koide, Y.; Asano, K.; Kawaguchi, M.; Matsushima, H.; Takenami, T.; Shinji, T.; Mori, M.; Tsuji, T., Formation of multicellular spheroids composed of adult-rat hepatocytes in dishes with positively charged surfaces and under other nonadherent environments. *Experimental Cell Research* 1990, 186, (2), 227-235.

76. Abu-Absi, S. F.; Friend, J. R.; Hansen, L. K.; Hu, W. S., Structural polarity and functional bile canaliculi in rat hepatocyte spheroids. *Experimental Cell Research* 2002, 274, (1), 56-67.

77. Fukuda, J.; Okamura, K.; Nakazawa, K.; Ijima, H.; Yamashita, Y.; Shimada, M.; Shirabe, K.; Tsujita, E.; Sugimachi, K.; Funatsu, K., Efficacy of a polyurethane foam/spheroid artificial liver by using human hepatoblastoma cell line (Hep G2). *Cell Transplantation* 2003, 12, (1), 51-58.

78. Yamashita, Y.; Shimada, M.; Tsujita, E.; Shirabe, K.; Ijima, H.; Nakazawa, K.; Sakiyama, R.; Fukuda, J.; Funatsu, K.; Sugimachi, K., Efficacy of a larger version of the hybrid artificial liver support system using a polyurethane foam/spheroid packed-bed module in a warm ischemic liver failure pig model for preclinical experiments. *Cell Transplantation* 2003, 12, (2), 101-107.

79. Mizuguchi, T.; Mitaka, T.; Sato, F.; Mochizuki, Y.; Hirata, K., Paper is a compatible bed for rat hepatocytes. *Artificial Organs* 2000, 24, (4), 271-277.

80. Mooney, D. J.; Park, S.; Kaufmann, P. M.; Sano, K.; McNamara, K.; Vacanti, J. P.; Langer, R., Biodegradable sponges for hepatocyte transplantation. *Journal of Biomedical Materials Research* 1995, 29, (8), 959-965.

81. Kaufmann, P. M.; Heimrath, S.; Kim, B. S.; Mooney, D. J., Highly porous polymer matrices as a three-dimensional culture system for hepatocytes. *Cell Transplantation* 1997, 6, (5), 463-468.

82. Powers, M. J.; Janigian, D. M.; Wack, K. E.; Baker, C. S.; Stolz, D. B.; Griffith, L. G., Functional behavior of primary rat liver cells in a three-dimensional perfused microarray bioreactor. *Tissue Engineering* 2002, 8, (3), 499-513.

83. Harada, K.; Mitaka, T.; Miyamoto, S.; Sugimoto, S.; Ikeda, S.; Takeda, H.; Mochizuki, Y.; Hirata, K., Rapid formation of hepatic organoid in collagen sponge by rat small hepatocytes and hepatic nonparenchymal cells. *Journal of Hepatology* 2003, 39, (5), 716-723.

84. Gerlach, J. C.; Schnoy, N.; Encke, J.; Smith, M. D.; Muller, C.; Neuhaus, P., Improved hepatocyte in-vitro maintenance in a culture model with woven multicompartment capillary systems - electron-microscopy studies. *Hepatology* 1995, 22, (2), 546-552.

85. Sakai, Y.; Naruse, K.; Nagashima, I.; Muto, T.; Suzuki, M., Large-scale preparation and function of porcine hepatocyte spheroids. *International Journal of Artificial Organs* 1996, 19, (5), 294-301.

86. Khetani, S. R.; Bhatia, S. N., Microscale culture of human liver cells for drug development. *Nature biotechnology* 2008, 26, (1), 120-126.

87. Mitaka, T.; Sato, F.; Mizuguchi, T.; Yokono, T.; Mochizuki, Y., Reconstruction of hepatic organoid by rat small hepatocytes and hepatic nonparenchymal cells. *Hepatology* 1999, 29, (1), 111-125.

88. Low, S. P.; Williams, K. A.; Canham, L. T.; Voelcker, N. H., Evaluation of mammalian cell adhesion on surface-modified porous silicon. *Biomaterials* 2006, 27, (26), 4538-4546.

89. Novikoff, P. M.; Cammer, M.; Tao, L.; Oda, H.; Stockert, R. J.; Wolkoff, A. W.; Satir, P., Three-dimensional organization of rat hepatocyte cytoskeleton: Relation to the asialoglycoprotein endocytosis pathway. *Journal of Cell Science* 1996, 109, 21-32.

90. Galarneau, L.; Loranger, A.; Gilbert, S.; Marceau, N., Keratins modulate hepatic cell adhesion, size and G1/S transition. *Experimental Cell Research* 2007, 313, (1), 179-194.